Measurement of the inclusive antineutrino cross section and ratio to neutrino cross section as a function of muon kinematics at $< E_\nu > \sim 6$ GeV on CH at MINERνA

Maria Mehmood

A THESIS SUBMITTED TO THE FACULTY OF GRADUATE STUDIES IN PARTIAL FULFILLMENT OF THE REQUIREMENTS FOR THE DEGREE OF MASTER OF SCIENCE

GRADUATE PROGRAM IN PHYSICS
YORK UNIVERSITY
TORONTO, ONTARIO

October 2024

I. ABSTRACT

This thesis will present a measurement of the inclusive antineutrinos cross section, in terms of muon kinematics, on the hydrocarbon tracker region of the MINERvA detector. The MINERvA experiment uses an on-axis flux peaking at 6 GeV from the NuMI beamline at Fermilab. An inclusive measurement in terms of muon kinematics will make for a comparatively easier comparison to model predictions, as such a measurement reduces the need for an accurate prediction of hadronic activity, which is harder to model.

Furthermore, muon kinematics are easier to reconstruct in the detector and a two-dimensional measurement yields a more detailed view of the phase space being explored. The measured cross section can be compared to the baseline model broken down by the predicted interaction channel. Some channels dominate in certain parts of phase space and will motivate which aspects of the model require more improvement.

This measurement is extracted in antineutrino mode as long-baseline neutrino oscillation experiments rely on a high precision understanding of both neutrino and antineutrino nucleus interactions.

CONTENTS

LIST OF TABLES

LIST OF FIGURES

II. INTRODUCTION

Neutrinos are the second most abundant particles in the universe, after photons. Photons are massless and travel at the speed of light, also known as nature's speed limit. Neutrinos cannot travel at the speed of light because they are not massless, but are very close to being massless. The Standard Model of Particle Physics incorrectly predicts neutrinos as being massless, and therefore, the discovery that neutrinos have mass, is indicative of physics beyond the Standard Model. There are three types of neutrinos: electron neutrinos, muon neutrinos, and tau neutrinos. The type of the neutrino is determined by observing the type of the final state lepton in a charged current neutrino interaction. For instance, a muon is observed in the final state when a muon neutrino interacts, and an electron is observed when an electron neutrino interacts. This is in addition to the other particles that get observed as a result of the interaction.

The anti matter counterpart of an electron is a positron, and the anti matter counterpart of a muon is a positively charged muon. Hence, when antineutrinoss interact, the anti matter counterparts of the charged leptons are observed. Therefore, muon neutrinos produce a negatively charged muon in the final state of a charged current interaction, and muon antineutrinoss produce a positively charged muon in the final state. In this way, neutrino interactions can be distinguished from antineutrinos interactions.

Neutrino oscillation is a phenomena that is not predicted by the Standard Model of Particle Physics. The observance of atmospheric neutrino oscillations [8] has motivated accelerator-based experiments to study the same oscillations, using GeV neutrinos, and hundred to thousand kilometers of baseline. Atmospheric neutrinos are produced when cosmic rays, which are primarily protons, collide with the Earth's atmosphere. As a result of these collisions, pions and kaons get created which then decay to neutrinos and muons. Atmospheric neutrinos get created naturally and continuously in the Earth's atmosphere. Accelerator neutrinos are produced in controlled beams, and can be tuned to produce a high flux of one particular type of neutrinos. The muons decay to muon and electron neutrinos. Hence, atmospheric neutrinos and accelerator neutrinos are a mix of muon neutrinos, as well as some electron neutrinos. Accelerator neutrinos are important because a beam of mainly muon neutrinos at higher energies can be created and used, as opposed to using lower energy, higher different flavour contamination, atmospheric neutrinos.

It is important to understand neutrino cross sections in the few GeV range. From FIG. 1, it is visible that in the few GeV range of energies, there are mainly three types of neutrino interactions: quasi elastic, resonance, and inelastic scattering in both neutrino mode and antineutrinos modes. The MINERvA experiment is sensitive to this range of energies and hence, extracts cross section measurements, to improve neutrino nucleus interaction models for oscillation experiments. The NOvA (NuMI Off-axis ν_e Appearance) experiment, a current neutrino oscillation experiment, found that cross section uncertainties make up $30-50\%$ of the systematic uncertainty on the most important oscillation parameter measurements [9].

Neutrino beams contain neutrinos with a range of energies. Hence, when a neutrino is detected, it is not known how much energy it had. To determine this, it is important to understand how it interacted. Neutrino interactions are complicated and work is required on models to entirely describe them. Modeling neutrino nucleus interactions accurately poses one of the biggest challenges for neutrino oscillation experiments to achieve the precision that is required.

It can be difficult to interpret cross section measurements because of nuclear effects. Therefore, there are models of neutrino nucleus interactions on bare nucleons and the effects of the nucleus are added to those. This makes it imperative to understand the effect of nuclear effects on cross section measurements. An effective way to do this is to make simultaneous cross section measurements of the same neutrino interaction process on various nuclei, and then study how the cross section scales with A. [10].

The number of events seen in a detector is equal to the product of the cross section of the process being measured, the incident flux, and the number of targets in the detector. Hence, the cross section is extracted by normalizing the number of neutrino events observed in the detector by the flux and the number of targets. Arriving at a true event rate in the detector requires using models to subtract off backgrounds and account for detector smearing as well as correct for the efficiency of the detector. The efficiency is the ratio of reconstructed events to true signal events. Background events are events that get reconstructed as signal, but originate from other processes. One way in which this can happen is, for example, the charge of the muon getting reconstructed incorrectly, causing a neutrino interaction to appear as an antineutrinos interaction.

Neutrinos are particles that only interact via the weak force. Hence, the interaction is

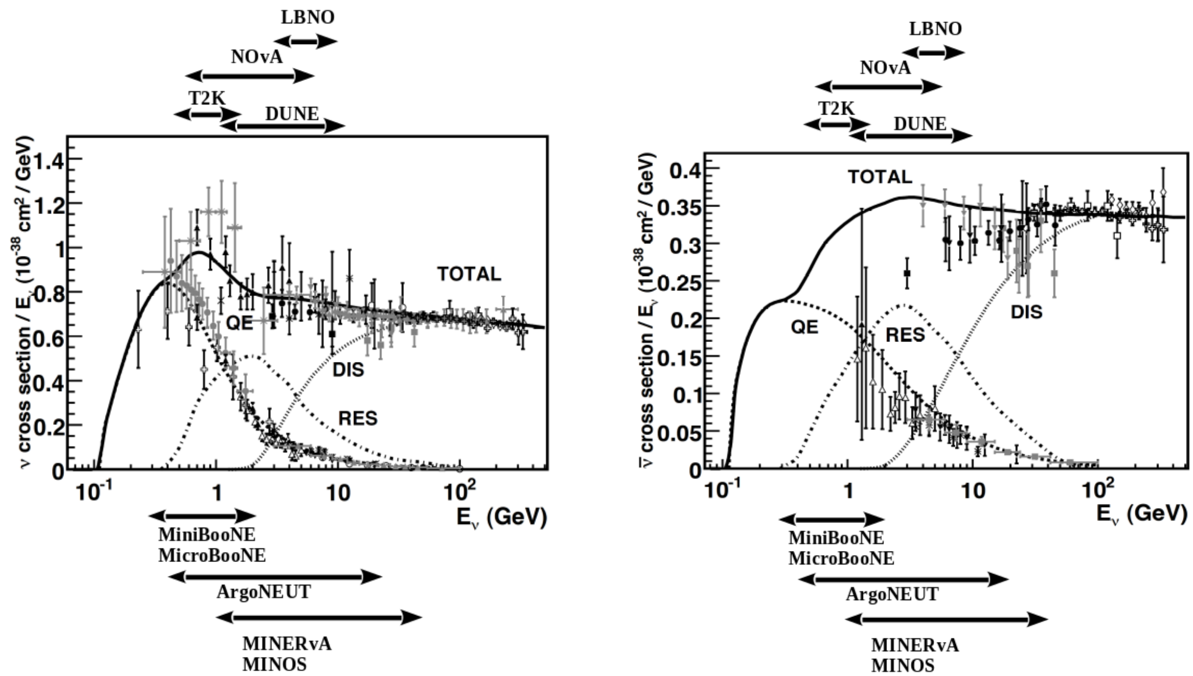

(a) (b)

FIG. 1. The neutrino cross section per neutrino energy is shown on the left and the corresponding antineutrinos plot on the right. The neutrino interaction channels are shown and the neutrino energy ranges to which various neutrino experiments are sensitive are marked [1].

mediated by the exchange of a massive W or Z boson. Neutral current interactions are mediated by the Z boson and constitutes interactions in which a neutrino stays a neutrino. Interactions mediated by a W boson are referred to as charged current interactions because they involve the transfer of electric charge since the W bosons are either positively or negatively charged, whereas the Z boson in neutral [11]. Charged current neutrino interactions are easier to detect because they yield a charged lepton in the final state.

The energy transferred by a neutrino dictates which interaction it is most likely to participate in. Low energy transfer usually happens at the nucleon level, whereas higher energy transfer is more likely to result in probing the nucleus at the quark level, as seen in FIG. 2. Quasi elastic interactions are characterized by an (anti)neutrino interacting on a nucleon to produce the corresponding outgoing lepton and new nucleon which conserve charge and lepton number. Resonance interactions require a neutrino with higher energy than what is required for a quasi elastic interaction as a resonance gets created in this type of interaction which then decays to a pion and a nucleon. Deep inelastic scattering occurs when the momentum transferred is so large that (anti) neutrino interactions happen at the quark level. These types of interactions are the most difficult to reconstruct because of most of the incoming neutrino energy going into the hadronic system of the interaction products.

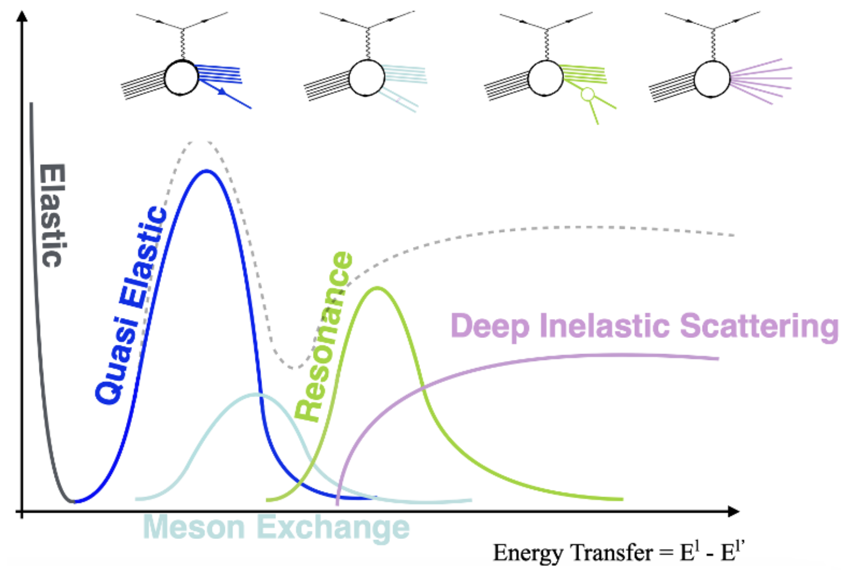

FIG. 2. The various interaction modes that dominate depending on the energy transferred in neutrino nucleus interactions [2].

.

In a nutshell, the MINERvA experiment extracts cross section measurements to improve cross section models and reduce the associated uncertainties for oscillation experiments. Moreover, the high statistics collected mean that many measurements are limited by systematic uncertainties instead of being statistically limited. Techniques are deployed for constraining systematic uncertainties and reducing them. Improved cross section models will aid in working towards lower uncertainties for neutrino oscillation experiments. The Deep Underground Neutrino Experiment (DUNE), which uses an accelerator based beam to get to the underlying physics, has a goal of 2% uncertainties on its measurements [12].

There are many questions that remain to be answered about neutrinos. The next generation neutrino oscillation experiments provide a promising outlook on answering more outstanding questions, provided the required precision is achieved.

Measuring neutrino oscillation in long baseline experiments can tell us about the neutrino mass ordering, and Charge Parity (CP) violation. These will not only advance the knowledge frontier, but may potentially resolve some mysteries of the universe, like why the universe is dominated by matter. We want to measure muon neutrino to electron neutrino oscillations, as well as muon antineutrino to electron antineutrino oscillations, which are hard to do with atmospheric neutrinos.

Hence, aiding in improving cross section models, by extracting cross section measurements, is an essential step for advancing neutrino physics.

This analysis is a two-dimensional inclusive cross section measurement of antineutrinoss on hydrocarbon in terms of muon kinematics. The same measurement is also extracted for neutrinos interacting on hydrocarbon and then the neutrino to antineutrinos cross section ratio is produced. The measurement is presented as a function of muon transverse and longitudinal momenta because these variables do not require reconstruction of the hadronic energy and are therefore, less model dependent. The muon longitudinal momentum serves as a proxy for the neutrino energy. The muon transverse momentum is a proxy for the four-momentum squared transferred to the nucleus. Earlier, cross section measurements were extracted in terms of neutrino energy and four-momentum squared transferred to the nucleus as models are constructed in terms of these variables. However, the large uncertainties associated with reconstructing the hadronic energy yielded less precise measurements. Hence, it is useful to extract more precise cross section measurements in terms of muon kinematics.

The event rate is what is seen in the detector and from that the cross section is extracted by accounting for various different factors. The equation for extracting a double differential cross section measurement is as follows:

$$\left(\frac{d^2\sigma}{d_x d_y}\right)_\alpha = \frac{\Sigma_j U_{j\alpha}(N_{data,j} - N^{bkgd}_{data,j})}{A_\alpha(\Phi T)(\Delta x)(\Delta y)} \tag{1}$$

$\left(\frac{d^2\sigma}{d_x d_y}\right)_\alpha$ is the double differential cross section in true bin α

$(N_{data,j} - N^{bkgd}_{data,j})$ is the background subtraction step

$U_{j\alpha}$ represents the unfolding from reconstructed bin j to true bin α

A_α represents efficiency correcting

(ΦT) represents normalizing by the flux and the number of targets

$(\Delta x)(\Delta y)$ represents normalizing by the bin

The next chapters in this thesis describe the ingredients for making this measurement, in particular, the neutrino flux (chapter 2), the MINERvA and MINOS detectors (chapter 3), and in chapter 4 the simulations we use of both the neutrino beamline, the detector, and the neutrino interactions themselves are described. Chapter 5 describes the analysis that extracts the cross section, Chapter 6 describes the uncertainties associated with the measurement, Chapter 7 describes the cross section results, and finally Chapter 8 provides comparisons between these results and several different models of neutrino interactions that are currently in use in the community. In this thesis, neutrino will mean neutrino and antineutrinos, unless otherwise specified.

III. THE NEUTRINO FLUX

The Neutrinos at the Main Injector (NuMI) beamline [3] provides both the neutrino and antineutrinos beams used in the MINERvA experiment. The simulated flux from each beam is shown in FIG. 3. The flux in neutrino mode per incoming proton was higher and less contaminated than the flux in antineutrinos mode.

The (anti) neutrino beam is created by crashing 120 GeV protons on a graphite target. The hadrons that are created are then focused in the forward direction by the magnetic horns, towards a 675m long decay region. Pions with a positive charge are focused for a neutrino beam or pions with a negative charge are focused for an antineutrinos beam. The hadrons then decay into (anti) neutrinos in the long decay pipe. The charged muons from these same decays are absorbed in the rock upstream of the detector and the result is a beam of mostly (anti) neutrinos. The beamline schematic can be seen in FIG. 4.

IV. THE MINERVA EXPERIMENT

This chapter will provide an introduction to the MINERvA experiment, by describing the detector design, the optical system, and muon reconstruction in detail. The MINERvA experiment measures cross sections of neutrino nucleus interactions using a variety of target materials.

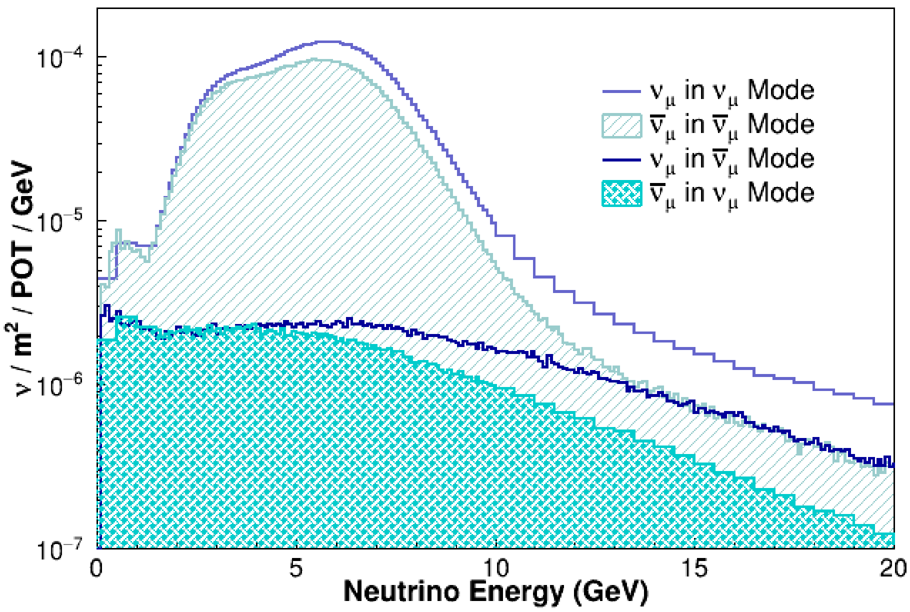

FIG. 3. This is the Medium Energy flux produced by the Neutrinos at the Main Injector (NuMI) beamline. The Medium Energy flux peaks at 6 GeV. The fluxes for running the beam in neutrino mode and antineutrinos mode are both shown, alongside the wrong sign contamination in each beam.

.

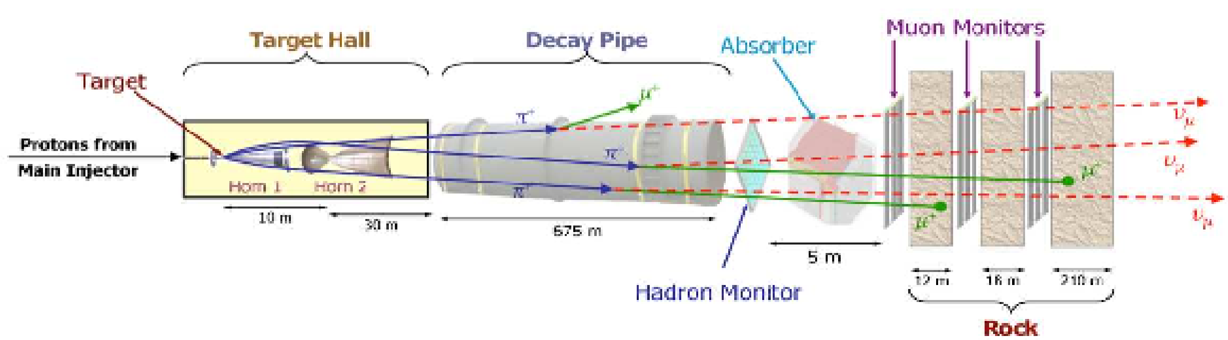

FIG. 4. This is a schematic of the NuMI beamline [3].

.

A. The MINERvA Detector Design

The MINERvA detector is a fine grained scintillator detector. It has nuclear passive target planes, interspersed with scintillator planes, located upstream of the active tracker region. The active tracker region is comprised of all hydrocarbon scintillator planes. The measurement for this analysis is made in the active tracker region. Electromagnetic and hadronic calorimeters surround both the passive target and hydrocarbon planes as in FIG. 6.

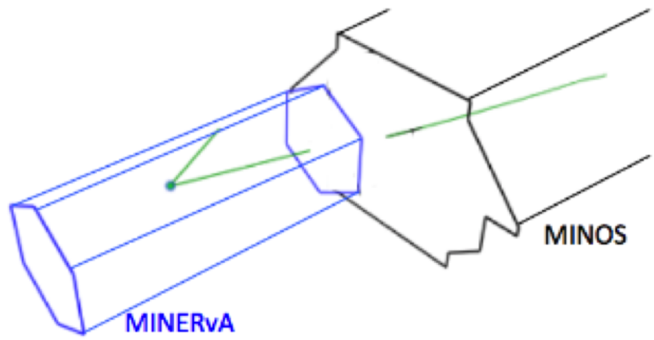

FIG. 5. A schematic of a muon track being matched between the MINERvA and MINOS detectors [4]

.

The MINOS experiment [13] is a neutrino oscillation experiment and has two detectors. The MINOS Near Detector is 2m downstream of MINERvA. MINERvA uses the MINOS Near Detector as a muon spectrometer for measuring the momentum and charge of the muons that exit the MINERvA detector upstream as in FIG. 5.

The MINOS Near Detector is a detector made of steel plates and instrumented with solid scintillator planes. can be used to identify the charge of charged particles as it has a magnetic field and the direction of the bending in the magnetic field identifies the charge. In the MINOS Near Detector, there is an aluminum coil in the direction of the beam, and the entire length of the detector. A 1.3 T toroidal field is generated in the detector due to a current of 40000 A-turns in the coil. There are 48 turns in the coil that each carry a current of 833 A. The coil has a 1.5 m distance from the beam center, as can be seen in FIG. 7. The magnetic field that is generated is sufficient to cause charged particles to bend and the radius of curvature is also a method of determining the particle's momentum.

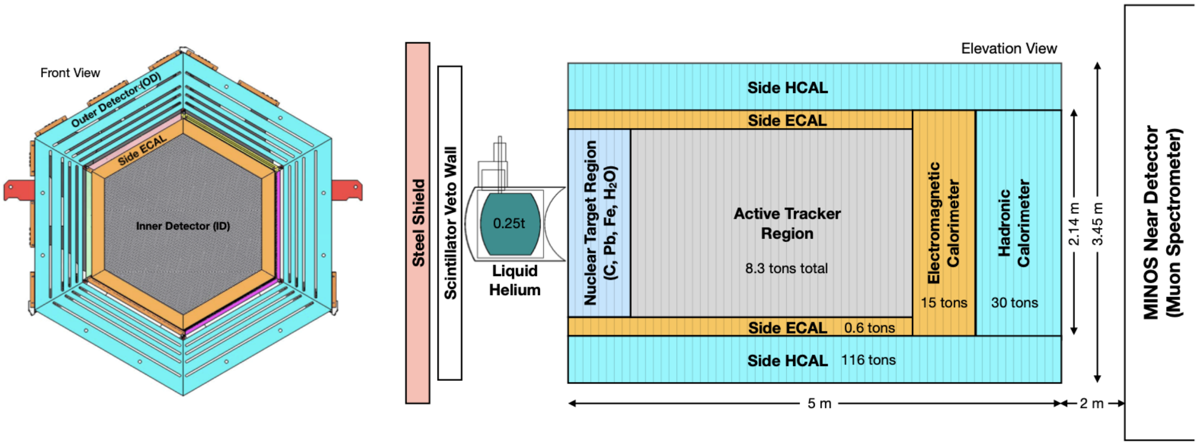

FIG. 6. On the left is a front view of a detector plane. On the right is a sideview of the MINERvA detector [5]

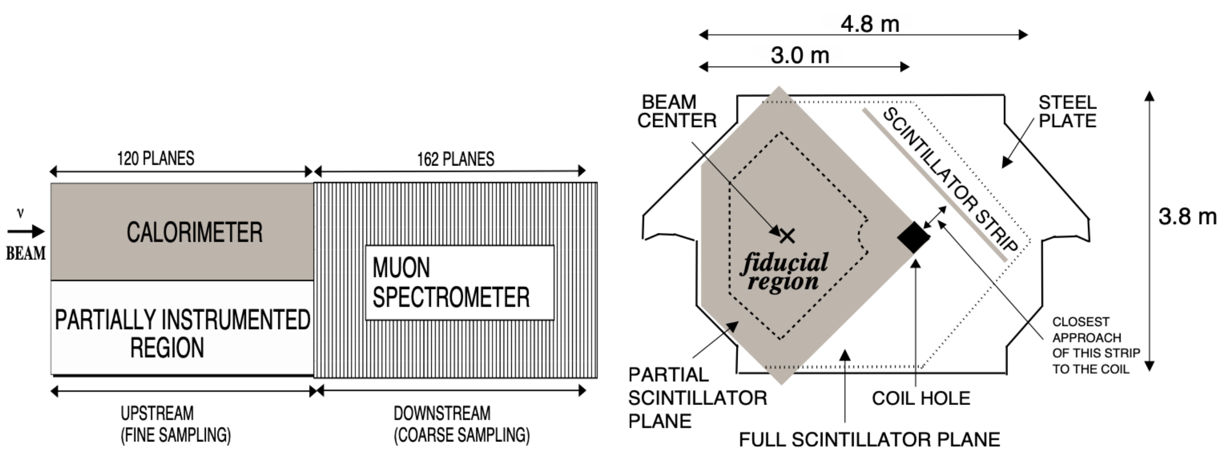

FIG. 7. On the left is the sideview of the MINOS detector. On the right is a front view of the two MINOS scintillator plane configurations [6].

B. The Optical System

When a charged particle travels through a scintillator strip, it creates light, and this light is then transmitted through a wavelength-shifting fiber to a photomultiplier tube (PMT). Each PMT has 64 channels and the light is transmitted to one of those channels. There are 507 PMTs installed on the MINERvA detector. Mounted on top of the PMTS are front-end electronic boards, which then process the signal from the PMTs. MINERvA has 32000 scintillator strips, each with a hole passing through it, and the wavelength-shifting (WLS) optical fiber going through the hole, as can be seen in FIG. 8.

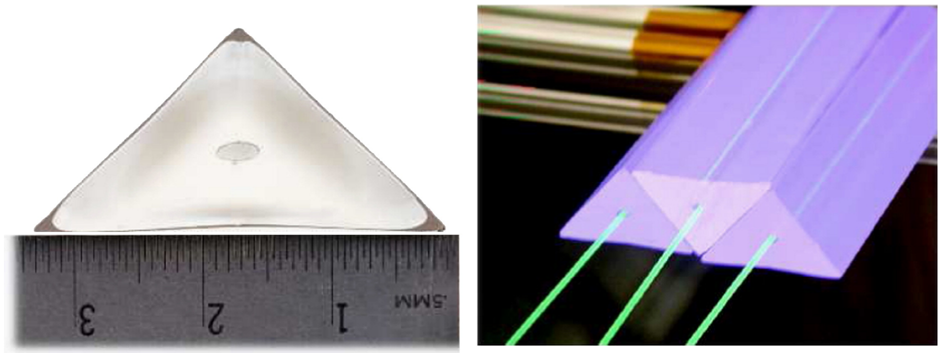

FIG. 8. The inner detector scintillator strips with the wavelength shifting fibers going through them [5].

.

C. Muon Reconstruction

An energy deposit left in the detector is termed a 'hit' and is the most rudimentary ingredient required for event reconstruction. The NuMI beam line [3] supplies a beam of neutrinos in what are called spills. A spill is a burst of beam provided over a 10 μs timing window. MINERvA reads out the entire detector for 16 μs for every 10 μs beam spill. This is because it also wants to capture any delayed detector activity, for example, from michel electrons from muon decays [14]. A michel electron is an electron produced from a muon decay, when the muon is at rest. The energy spectrum of these electrons is well defined and at an energy corresponding to half the muon mass, 105.66 MeV [15], there is a sharp cut off in the electron's energy distribution [16].

The protons on target (POT) for each spill range from 2-5 times 10^{13}. The integrated POT quantifies the time duration for which the detector was exposed to the beam, and how POT/spill determines how intense the beam was. This is because it is the number of protons on target which refers to the number of protons collided on the NuMI beam target to create the neutrino beam. Hence, the greater the POT, the higher the number of scattering events that are expected. The monte carlo simulation samples that are plotted in this thesis have been normalized to the number of POT collected in the data [17].

For each NuMI beam spill, the hits collected in that spill are grouped into time slices corresponding to individual neutrino interactions. Each time slice is then analyzed to combine hits into clusters based on the hits being contained in the same scintillator plane and being adjacent to each other in strip space. The cluster time corresponds to the time of the highest energy hit. The cluster position is the energy-weighted average of the various hit positions in the strip [5]. The timing resolution per hit is about 3 ns.

Muon reconstruction begins as track reconstruction. Each time slice is analyzed in order to collect clusters into 'seeds'. There are three possible orientations of a plane: X, U, V to enable three dimensional reconstruction. A seed contains three clusters in adjacent planes of the same orientation (X, U, or V) which fit to a straight line. Seeds are then connected to form track candidates. Three dimensional reconstructions of the tracks are obtained by repeating the merging of seeds in each of the three orientations: X, U, and V. A Kalman filter routine [18], [19] is used to obtain fits to create the tracks and enables tracks to be extrapolated through planes with dense activity, such as in the case of a hadronic shower. The Kalman filter fit results are used to determine if any cluster is missing from a track, in which case it is added to the track. First, for both the start and end positions of the track, the fitted track is projected in both the downstream and upstream directions to scan for any unused clusters it may be crossing. In this way, the unused clusters are added to the track.

As there can be multiple particles that are associated with an 'event', which is an entire neutrino interaction, the track finding procedure is repeated until there are no more tracks to be found for particles associated with a particular event.

Tracks are matched between the MINERvA detector and the MINOS Near Detector in order to completely reconstruct the muon track, as in FIG. 5. The kinetic energy lost due to the particle's range in the MINERvA detector is combined with the momentum reconstructed in the MINOS detector to completely reconstruct the muon momentum at the point the muon was created. The MINOS detector reconstructs the muon momentum by either range or curvature. In order to reconstruct by range, the reconstructed track in the detector is used alongside the Bethe Bloche equation. In order to reconstruct by range, the track needs to end in the MINOS detector, otherwise we can also reconstruct by curvature [20]. The muon charge is determined by the direction of its bending in the MINOS detector.

MINERvA used a web-based event viewer called Arachne to create event displays for looking at events as well [21]. An example of an event display can be seen in FIG. 9.

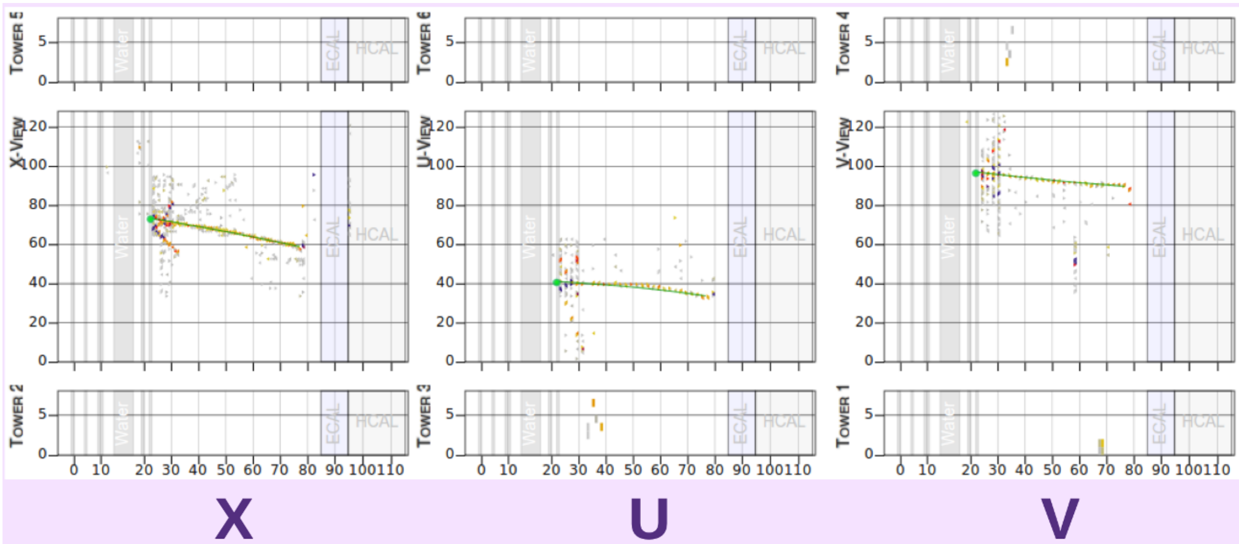

FIG. 9. An Arachne event display showing different views of the planes, used to reconstruct events [7]

V. THE SIMULATION

A. Neutrino Beam Flux Simulation

GEANT4 [22] is a software that simulates the passage of particles as they travel through matter. A GEANT4-based simulation is used for the NuMI beamline to predict the neutrino and antineutrinos fluxes. Hadron production data available from the NA49 experiment of measurements of 158 GeV protons on carbon [23] is used to improve the GEANT4-based simulation by reweighting it as a function of pion kinematics. Similarly, other related data are also used to improve the simulation. Furthermore, the flux prediction is constrained using neutrino electron elastic scattering events in the MINERvA detector, since the neutrino electron elastic scattering cross section is known accurately [24]. An even more stringent constraint is applied by combining this constraint with the constraint derived from antineutrinos electron scattering and inverse muon decay ($\nu_\mu + e^- \rightarrow \mu^- + \nu_e$) data [25]. The combined flux constraint reduces the flux uncertainty on the neutrino flux in the neutrino beam from 7.6% to 3.3% and the uncertainty on the antineutrinos flux in the antineutrinos beam from 7.8% to 4.7%.

B. Neutrino Event Generation

The GENIE neutrino event generator [26] version 2.12.6 is used for generating neutrino events. GENIE simulates neutrino events in the nucleus by starting with the initial neutrino interaction and includes the final state particles leaving the nucleus. GENIE assigns the identity and kinematics of each of the final state particles leaving the nucleus. GENIE simulates events for various different interaction processes using a probability based approach. The Llewellyn-Smith formalism [27] is used for simulating quasi-elastic interactions. Quasi elastic interactions yield a nucleon and a muon in the final state. The Rein-Sehgal model is used for simulating resonance production [28]. The Bodek Yang approach [29] is used for deep inelastic scattering (DIS) interactions.

The presence of the nucleus modifies the GENIE predictions as follows: The nucleus itself is simulated using the relativistic Fermi Gas model [30] with an additional Bodek-Ritchie high momentum tail [31] for nucleon nucleon short range correlations. Final state interactions of particles before they exit the nucleus are modeled using the INTRANUKE-hA package [32].

In addition to the baseline GENIE model, MINERvA has created some data driven modifications or "tunes" which are used on top of baseline GENIE to improve the interaction model. The random phase approximation (RPA) part of the Valencia model [33] [34] is used to improve the simulation of quasielastic events. The cross section of multi-nucleon scattering (two-particle two-hole) is increased for certain energies based on MINERvA data fits from the low energy data set taken before the data reported here [35]. The rate of 2p2h is created by 50% over the nominal prediction when integrated over all of phase space. The non-resonant pion production is decreased by 43% according to data fits to deuterium measurements [36]. Together, these corrections on top of GENIE 2.12.6 are referred to as MINERvA Tune v1.

GENIE passes the final state particles and their kinematics to the GEANT4-based program for simulating the track paths of the particles in the detector planes.

C. Detector Simulation

The MINERvA detector response is simulated using GEANT4 version 4.9.3.p6. A simulation is also done for the optical performance and the electronics performance [37]. A charged particle test beam impinging on a smaller version of the MINERvA detector determined the absolute energy response to charged hadrons [38].

VI. ANALYSIS

The following subsections will walk us through the steps for extracting a cross section. First, event reconstruction is done, followed by background subtraction, and then transferring from reconstructed variables to true variables by unfolding. After that, the distributions are efficiency corrected and then normalized by the flux and the number of targets to extract the cross section.

The analysis goal is to extract the two-dimensional inclusive cross section measurement of antineutrinoss interacting on hydrocarbon. An additional goal of this thesis is to re-extract the neutrino cross section [37] using the newer flux constraint [25], and compute the neutrino to antineutrinos cross section ratio.

A. Event Reconstruction

This is an inclusive measurement of charged current interactions extracted on hydrocarbon. The reconstruction cuts that were made include a 5σ significance muon curvature cut, a deadtime cut to remove events where the electronics were reading out previous activity in the spill, a muon charge cut, an 850 mm apothem cut on the xy vertex location, a z (location upstream or downstream in the detector) vertex tracker cut, and a 20 degrees muon angle cut. These reconstruction cuts picked out the sample of inclusive events on hydrocarbon, taking into account the physical limitations of the detectors, MINERvA and MINOS. For the antineutrinos cross section, all events with an anti muon in the final state are considered signal. For the neutrino cross section, all events with a muon in the final state are considered signal. This is because this is an inclusive analysis and so all charged current events are considered signal.

The DIS (Deep Inelastic Scattering) category is divided into two. True DIS events are characterized by the ones in which the invariant mass of the hadronic system is greater than 2.0 GeV/c^2 and the 4-momentum transferred squared is greater than 1.0 GeV^2/c^4. The remaining events are GENIE classifies as DIS are labeled as Soft DIS events.

This measurement is extracted in terms of muon kinematics, to reduce the model dependence, that comes with hadronic energy reconstruction. A two-dimensional measurement is performed so that a more detailed view of the phase space can be observed using the high statistics of the MINERvA experiment. In neutrino mode, 3.74 million events were reconstructed. In antineutrinos mode, 2.06 million events were reconstructed. The reconstructed events for each mode are shown in FIG. 10 and FIG. 11. The red curves represent the monte carlo prediction used which is MINERvA Tune v1, as described in Section IV. The red band around the red curve represents the total uncertainty on the monte carlo prediction. The data is reported with the statistical uncertainty shown. The error bars are very small on most data points, as the high statistics result in a small fractional statistical uncertainty in each bin. The predicted breakdown by interaction type is also provided in each bin. The multipliers help see the curves on a similar level on the plot. Higher multipliers correspond with fewer events in the particular bin.

The MINERvA tune v1 prediction has been tuned on earlier Low Energy (LE) era results. FIG. 10 shows that the MINERvA tune v1 has good agreement with the data except in the lowest and highest momentum bins. This could be because the interaction channels that dominate in these areas are less well understood, and also because of higher backgrounds in these areas. This two dimensional view of phase space enables us to pull apart which interaction channels dominate in which bins. For instance, deep inelastic scattering dominates at the highest momenta. Furthermore, making a measurement in terms of muon kinematics is useful because we measure muon kinematic well, since it comprises of reconstructing the tracks in the detector, and converting the light signal that was read in to the energy that was deposited in the detector. This doesn't depend on reconstructing hadrons and so is more robust.

B. Background Subtraction and Sideband Constraint

The reconstructed events are now background subtracted and the simulation is used to predict the level of backgrounds in the sample. Since, we don't want to rely entirely on

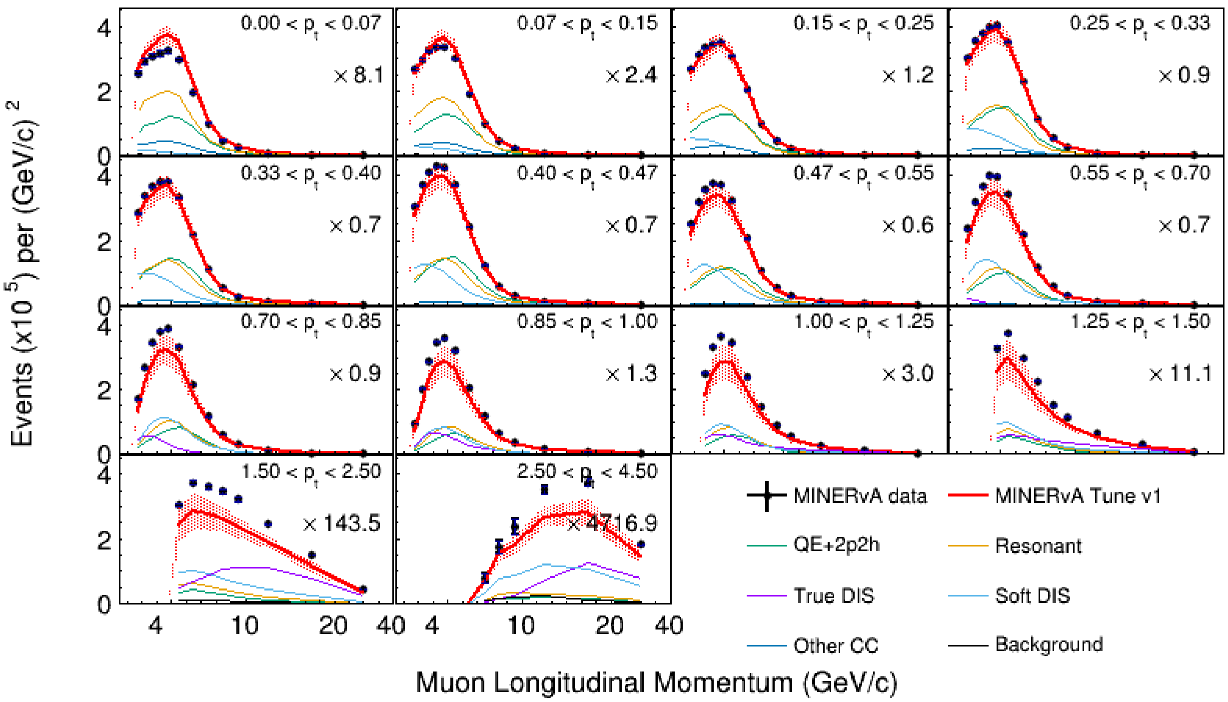

FIG. 10. The events reconstructed in antineutrinos mode, with the predicted breakdown by interaction channel.

the simulation as it can be not entirely accurate, we also use the data to constrain our background prediction by studying what is referred to as the sideband sample, which will be referred to after discussing the backgrounds.

The selected sample for this analysis in both neutrino and antineutrinos modes has a high purity. This is because an inclusive analysis in terms of muon kinematics, inherently has fewer backgrounds, than exclusive channels. The backgrounds are only a few percent of the reconstructed events and rise to 8-10% in the highest transverse muon momentum bins.

There are two types of background in this analysis: wrong sign and/or neutral current events. Wrong sign backgrounds correspond to neutrino events in the antineutrinos beam or vice versa. There are three ways in which neutrinos can appear in the antineutrino beam. First, hadrons can go through the neck of the horn and not get focused. Second, muon decay yields the wrong sign neutrino. Third, the neutral kaons in the beam don't get focused since they are neutral particles and they decay to muons or pions which then further decay.

Neutral current interactions contribute backgrounds because the pions from neutral current events can get mis reconstructed as muons in the MINOS near detector and hence, fake

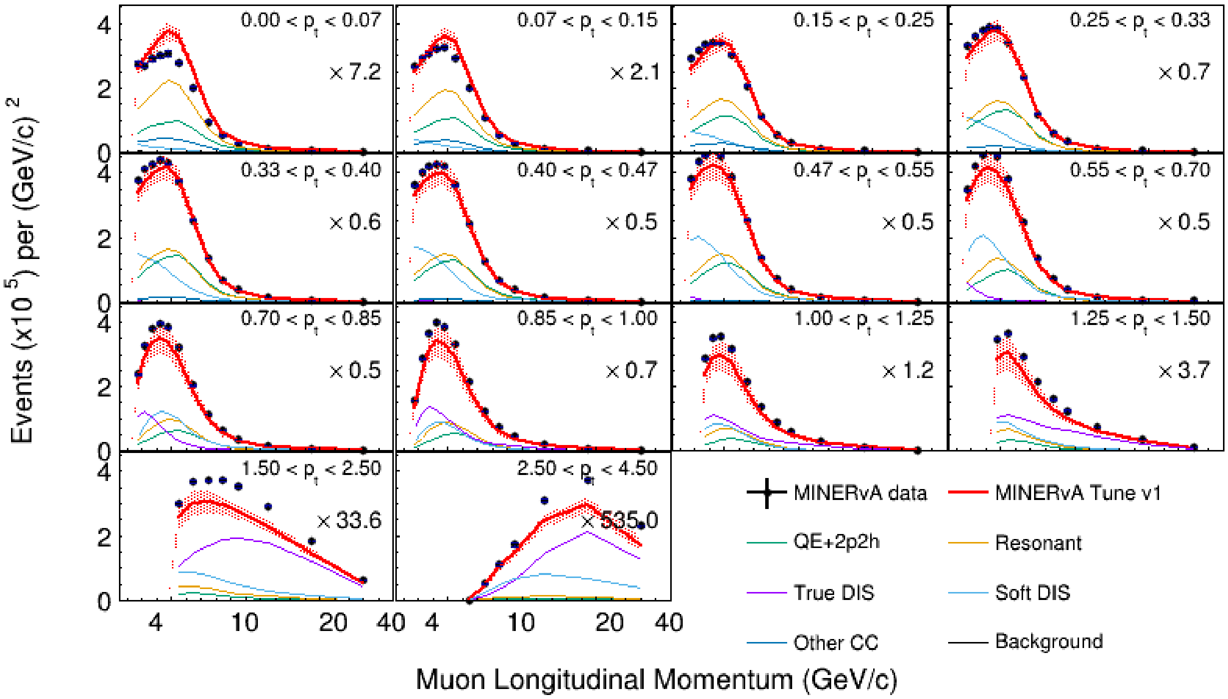

FIG. 11. The events reconstructed in neutrino mode, with the predicted breakdown by interaction channel.

a signal, though they were a neutral current event. For neutral current events, the neutrino scatters off the nucleon by exchanging a Z boson and yields a neutrino and the nucleon in the final state.

The helicity cut is applied to remove wrong sign events but there are events that get reconstructed with a muon charge and therefore passes the helicity cut. MINERvA Tune v1 is used to predict the amount of background. FIG. 12 and FIG. 13 show the background breakdown for each mode. In antineutrinos mode, wrong sign backgrounds dominate because neutrinos have a higher cross section. In neutrino mode, there is a sizable contribution from both neutral current and wrong sign backgrounds to the total background. Overall, there is a higher total background in antineutrinos mode than in neutrino mode.

The sideband study was done both in neutrino mode and antineutrinos mode to better constrain the background prediction. A sideband is a region of background that is looked at in greater detail as a mechanism of constraining the background prediction for the analysis in a data driven way. Hence, the discrepancy between the data and the monte carlo in the sideband region was studied. The wrong sign event sample was used as the sideband. The

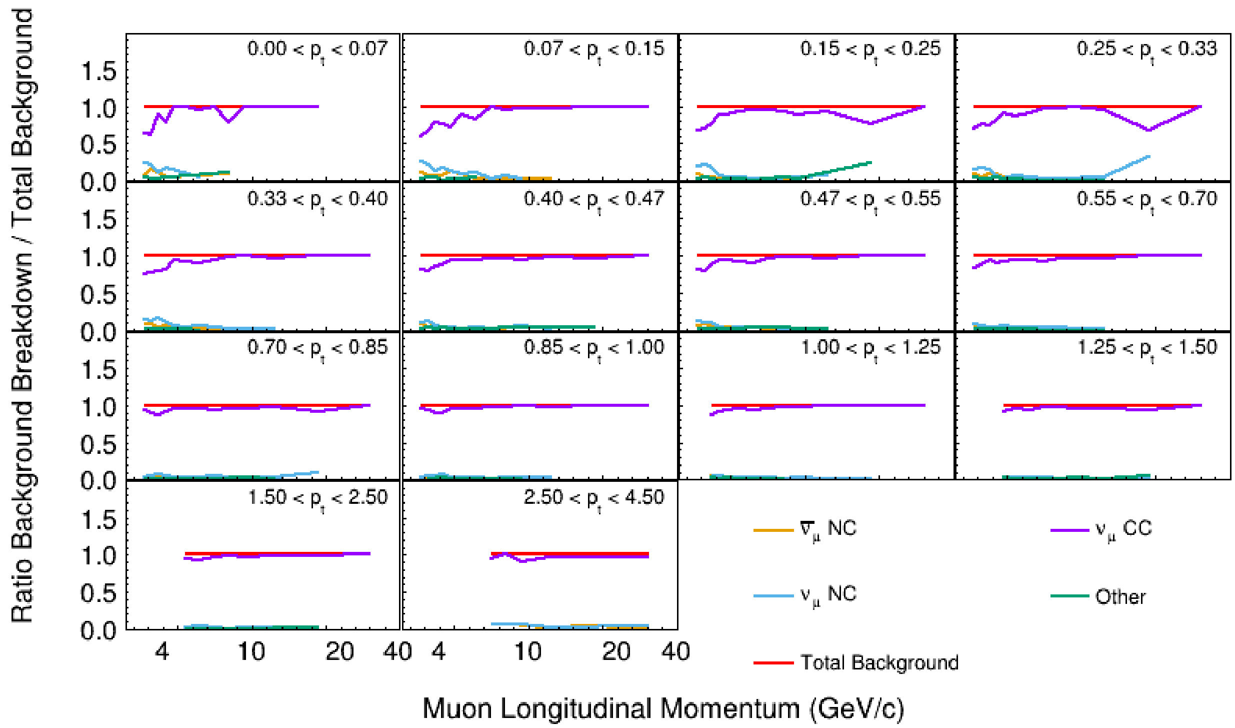

FIG. 12. Breakdown of the background in antineutrinos mode.

ratio of data to monte carlo is shown in FIG. 14 a) for antineutrinos mode. It is apparent that the monte carlo prediction doesn't agree with the data in almost all of the bins.

A correction factor is determined and the neutrino charged current and neutrino neutral current contributions to the background are scaled by the correction factor. The correction factor is the data to monte carlo ratio from FIG. 14 a) which is 1.33 in antineutrinos mode and 1.19 in neutrino mode. After applying the correction factor, the monte carlo agrees with the data as seen in FIG. 14 b). This demonstrates that the correction has better constrained our background prediction by achieving data and monte carlo agreement in the sideband region. Since it is the same correction factor being applied in all of the bins, the data to monte carlo discrepancy in the sideband region could be because of an overall mismodeling of particles bending away from the coil in the MINOS near detector, or an overall mismodelling of removing wrong sign pions in the NuMI beamline, for example.

The effect of tuning the background is very small and at the few percent level as can be seen in FIG. 15. This is because the level of backgrounds being subtracted off was very small in the first place since this is an inclusive analysis.

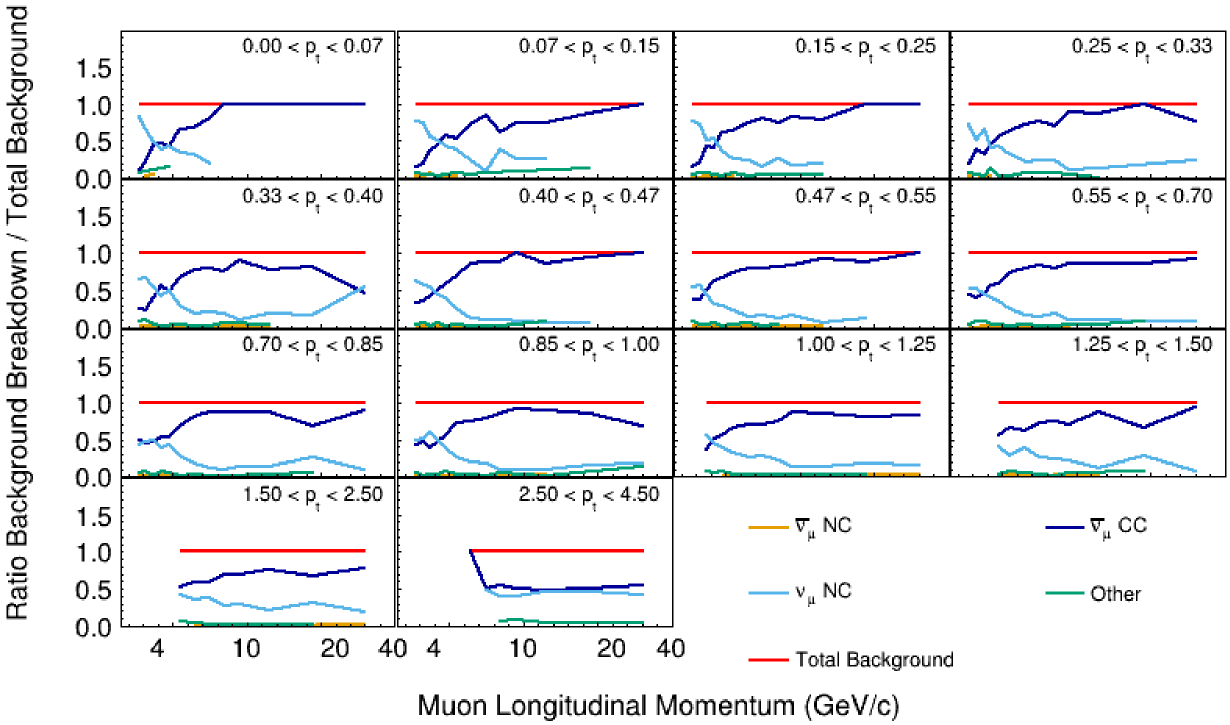

FIG. 13. Breakdown of the background in neutrino mode.

C. Unfolding

The background subtracted data is unfolded as part of the next step in extracting a cross section measurement. Unfolding is required to correct for detector smearing. The process of unfolding takes a smeared distribution to the corresponding true distribution. A migration matrix depicts the percentage of events that were generated in a true bin and the number of events in the corresponding reconstructed bin. The migration matrix for muon variables is mostly diagonal because of good reconstruction of muons in the detector as can be seen in FIG. 16. The migration matrix is not easily invertible and hence, the d'Agostini unfolding [39] [40] method is used to numerically invert the migration matrix. This method requires one to input the number of iterations to use while using the migration matrix to take a reconstructed distribution to the corresponding true distribution. The zeroth iteration corresponds to the reconstructed distribution not being unfolded at all. In order to determine the appropriate number of iterations to use, a warping study is conducted. For the monte carlo, both the reconstructed and true distributions are known. Hence, different warps are created for the monte carlo.

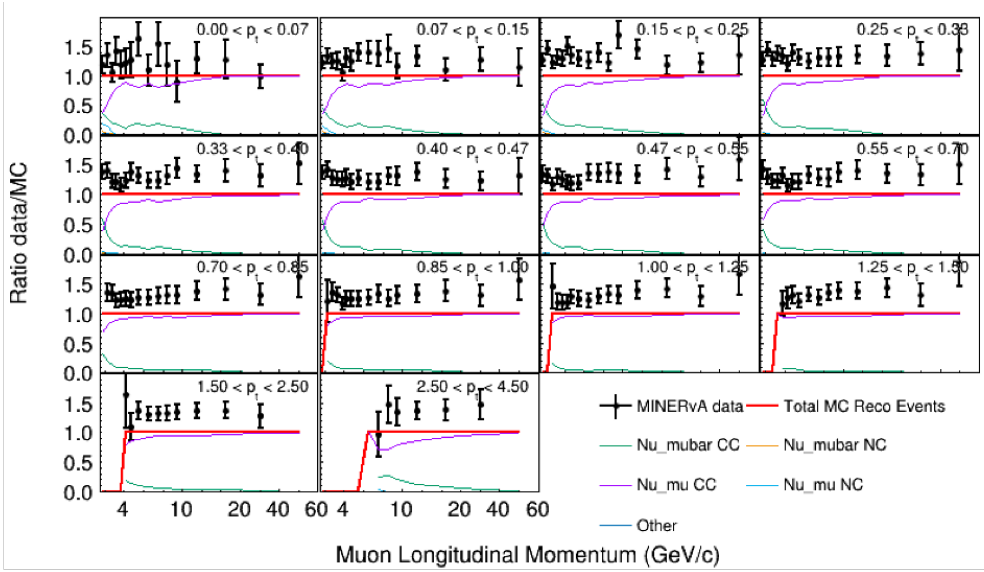

(a)

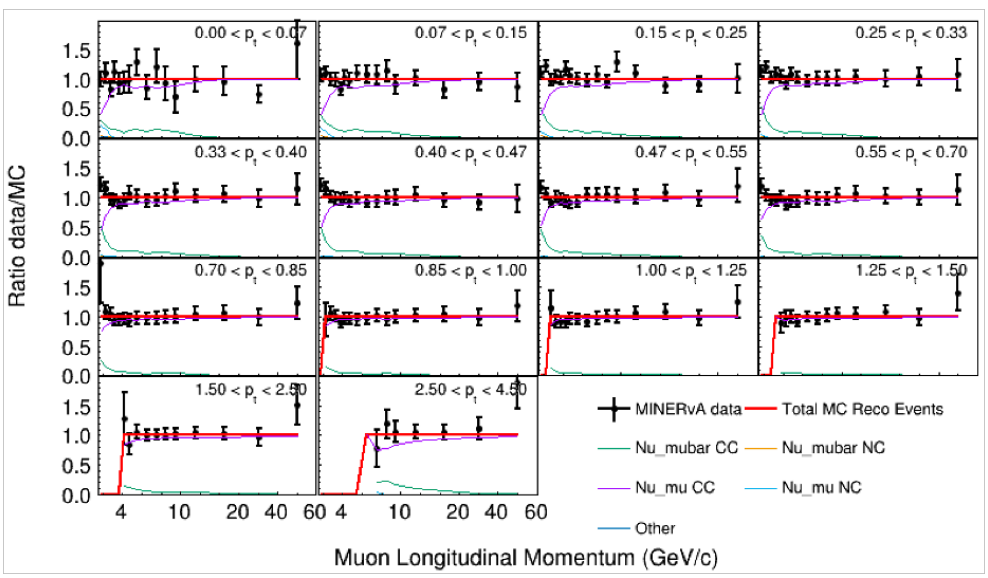

(b)

FIG. 14. a) The Data / MC ratio of the sideband sample in antineutrinos mode. b) The Data / MC ratio of the sideband sample in antineutrinos mode, after applying the correction to the neutrino CC and neutrino NC components of the background.

A warp is an altered monte carlo prediction from MINERvA Tune v1 by, for example, turning certain weights on or off. For instance, the non resonant pion reweight was turned off as a warp. The ratio of the warped distribution to the original distribution demonstrates the size of the warp as in FIG. 17 a). The goal is to use the MINERvA Tune v1 migration matrix to unfold the reconstructed warped distribution back to the true warped distribution.

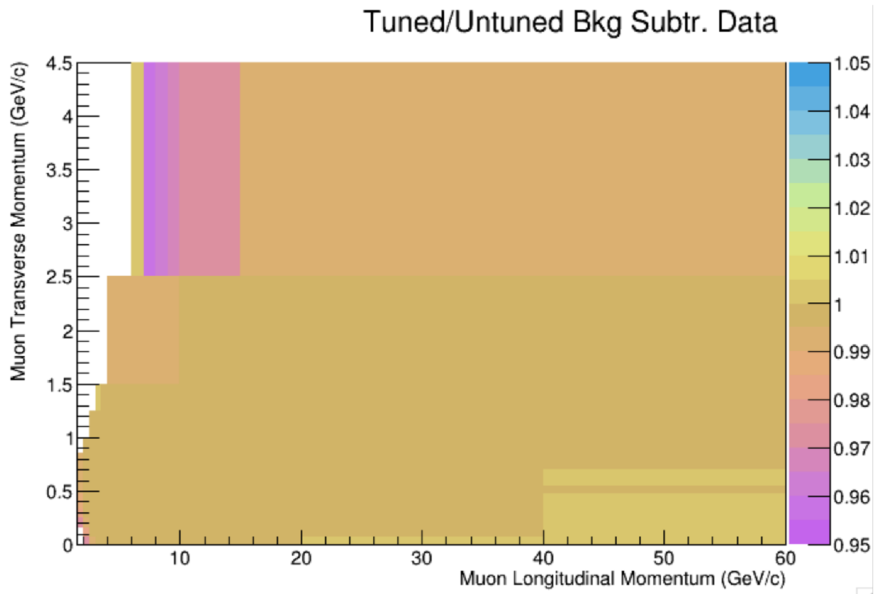

FIG. 15. The Tuned / Untuned background subtracted data in antineutrinos mode

.

The number of iterations that work for all of the warps used is then used for unfolding the reconstructed data distribution. However, very drastic warps larger than the observed data - monte carlo discrepancy were not used. The approach is to reduce the model dependence of the unfolding process by ensuring that many distributions with physics described by different underlying models can still be unfolded by the central value MINERvA Tune v1 migration matrix to arrive back at the true distribution from the reconstructed distribution. FIG. 17 b) demonstrates the appropriate number of iterations required for taking a reconstructed distribution to its true distribution. The warping study is done for various different warps to determine the number of iterations that should be used for the data. It was concluded that 10 iterations should be used for neutrino mode and antineutrinos mode both in the unfolding process.

D. Efficiency Correction

The background subtracted unfolded distributions are then efficiency corrected. This corrects for the signal events that occurred outside of the fiducial volume but were reconstructed to have happened inside the fiducial volume, as well as, events that occured in the fiducial volume but were mis-reconstructed as background events. The efficiency tends to

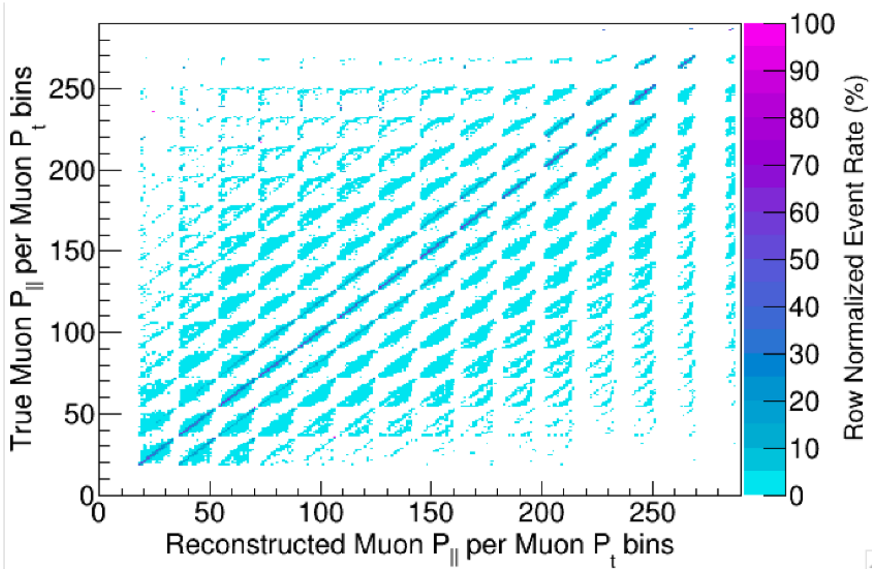

FIG. 16. The migration matrix for antineutrinos mode.

.

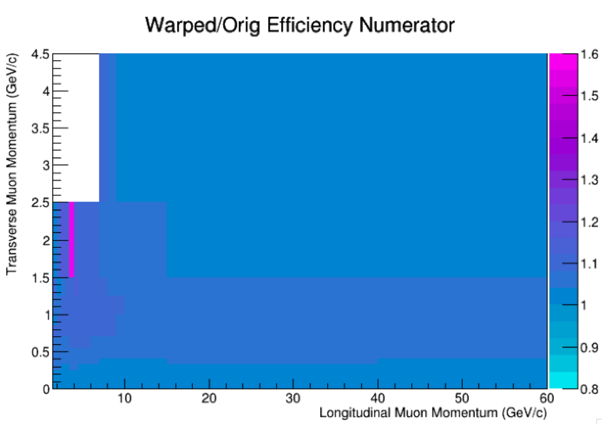

(a)

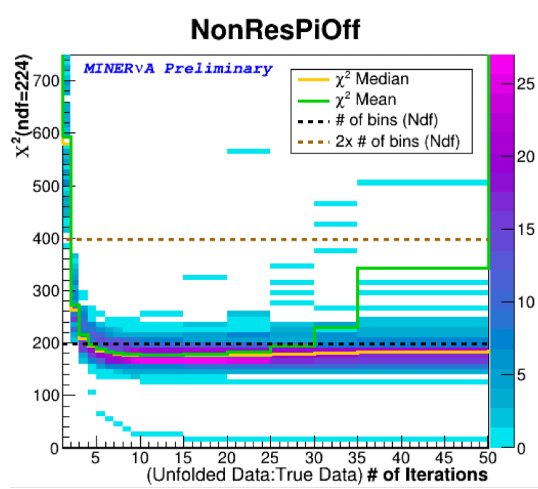

(b)

FIG. 17. a) The size of the warp for non resonant pion reweight turned off. b) The chi2 distribution versus the number of iterations for the non resonant pion reweight turned off warp.

fall off near the angle cut boundary as it is harder to reconstruct the events near the boundary. The efficiency plots look the same for neutrinos in neutrino mode and antineutrinoss in antineutrinos mode. FIG. 18 a) shows the efficiency for antineutrinoss in anti antineutrinos mode. FIG. 18 b) shows the efficiency for antineutrinoss in neutrino mode. The efficiency for antineutrinoss in neutrino mode is smaller because of considering the sample of muons

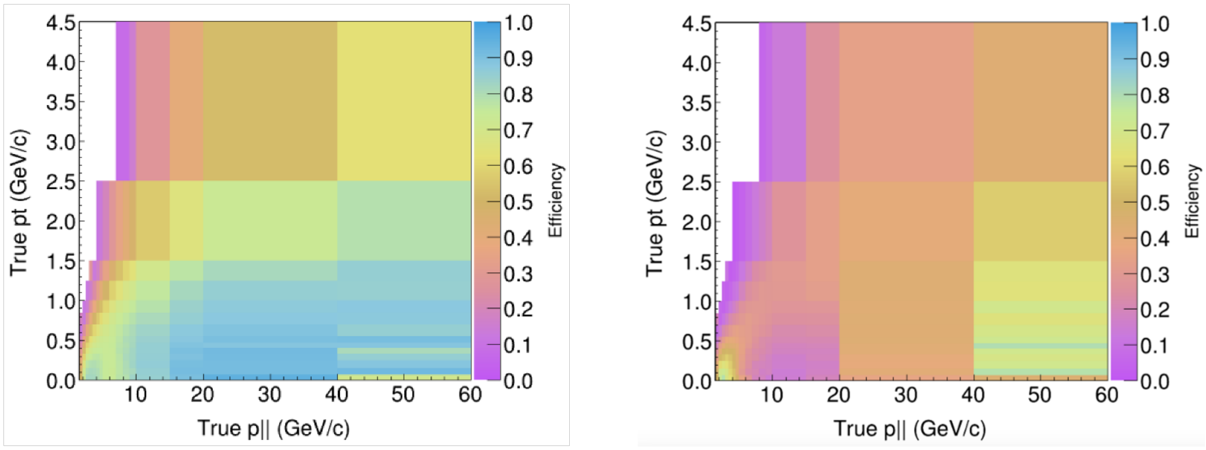

(a) (b)

FIG. 18. The efficiency for a) antineutrinoss in RHC b) antineutrinoss in FHC

that are bending away from the coil in the MINOS Near Detector. A lot of these particles leave the detector and hence, there are few measurements on them and consequently a lower efficiency.

VII. SYSTEMATIC UNCERTAINTIES

The next chapter will show the cross section result. It is useful to discuss the uncertainties on the cross section measurement first. There are several sources of systematic uncertainties associated with this measurement.

The equation for extracting a double differential cross section:

$$\left(\frac{d^2\sigma}{d_x d_y}\right)_\alpha = \frac{\Sigma_j U_{j\alpha}(N_{data,j} - N^{bkgd}_{data,j})}{A_\alpha(\Phi T)(\Delta x)(\Delta y)} \tag{1}$$

$\left(\frac{d^2\sigma}{d_x d_y}\right)_\alpha$ is the double differential cross section in true bin α

$(N_{data,j} - N^{bkgd}_{data,j})$ is the background subtraction step

$U_{j\alpha}$ represents the unfolding from reconstructed bin j to true bin α

A_α represents efficiency correcting

(ΦT) represents normalizing by the flux and the number of targets

$(\Delta x)(\Delta y)$ represents normalizing by the bin

From Eqn (1) it's clear that there are flux uncertainties, reconstruction uncertainties that would affect the unfolding, and neutrino interaction uncertainties which would affect the efficiency, along with normalization uncertainties that affect the number of targets in the detector. This chapter describes the different sources of uncertainties. The effects of systematic uncertainties on the cross-section measurement are evaluated by considering alternate universes in which a specific aspect of the experiment is varied by a certain amount for each universe, and the cross section is computed in each shifted universe.

The many universe method is used for determining systematic uncertainties on the cross section measurement. The systematic uncertainties are determined by considering alternate universes in which known parameters are varied by certain amounts and the cross section is computed in those alternate universes. The analysis cuts are applied in each universe and hence, it is possible that certain events fail the cuts in certain universes but pass them in other universes. For almost all of the systematic uncertainties, two universes are considered, which are varied by $\pm 1\sigma$ the parameter value. Hence, the cross section is computed in each shifted universe and then how different it is from the central value cross section determines the uncertainty due to the parameter that was shifted. The statistical and systematic uncertainties are combined in quadrature. This chapter describes the largest sources of uncertainty in this measurement.

A. Muon Reconstruction

The cross section is reported as a function of muon angle with respect to the neutrino beam. The Muon Reconstruction category includes uncertainties in muon angle and muon energy reconstruction. Therefore, an uncertainty in the angle of the beam translates into a muon reconstruction uncertainty. The uncertainty in the angle at which the beam is incident on the detector is captured as an uncertainty in the X and Y directions. The uncertainties are $\delta\theta_x = 0.001$ and $\delta\theta_y = 0.0009$ [41]. Furthermore, the muon energy resolution quantifies the error on the muon energy due to the $\pm 0.4\%$ difference in the resolution of muon energy between the simulation and the data. Finally, since part of the muon's momentum gets reconstructed in MINERvA and the remaining in MINOS, there are systematic uncertainties associated with both.

The muon momentum reconstructed by range in the MINOS detector incurs an uncertainty of $\pm 0.984\%$. The muon momentum reconstructed by curvature uses an uncertainty of $\pm 2.5\%$ for muon momentum less than 1 GeV, and $\pm 0.6\%$ for muon momentum greater than 1 GeV [42]. The higher energy muons will bend less in the magnetic field.

B. Flux

The flux uncertainty has been constrained by MINERvA measurements of neutrino electron scattering [25] to be 4.7% from 7.8% for the antineutrinos flux in the antineutrinos beam and to be 3.3% from 7.6% for the neutrino flux in the neutrino beam. The initial uncertainties come from uncertainties in hadron production measurements which affect initial pion momentum and angular distributions.

C. Models, Normalization, Hadronic Response

Neutrino interaction model uncertainties do not dominate in any muon transverse momentum or muon longitudinal momentum bin because the backgrounds are very small and few cuts are applied. The model uncertainties are most significant in the highest muon transverse bin because that is close to the angle cut boundary of phase space. Furthermore, the model uncertainties appear at the lowest and highest transverse muon momentum because that is where higher backgrounds appear as well.

The normalization uncertainty is very small and corresponds to the number of targets, 3.24e+30. There is also an uncertainty associated with the number of protons on target.

The hadronic response systematic is small for this analysis because hadrons are not reconstructed since this is an inclusive measurement as a function of muon kinematics. The hadronic response systematic uncertainty appears in the bins with more background because of reconstructing pions.

The breakdown of uncertainties on the antineutrinos cross section is shown in FIG. 19. The breakdown of uncertainties on the neutrino cross section is shown in FIG. 20. The main uncertainties are flux and muon reconstruction. The flux uncertainty is lower in neutrino mode because of the stronger flux constraint. The muon reconstruction uncertainty is similar in both modes because the charge of the muon doesn't impact how it gets reconstructed. The muon reconstruction uncertainty is higher around the focusing peak. The breakdown of uncertainties on the unweighted neutrino to antineutrinos cross section is shown in FIG. 21. There is cancellation of correlated systematics like the muon reconstruction, but not cancellation of the flux systematic, since the fluxes uncertainties are far less correlated due to the independent flux constraints.

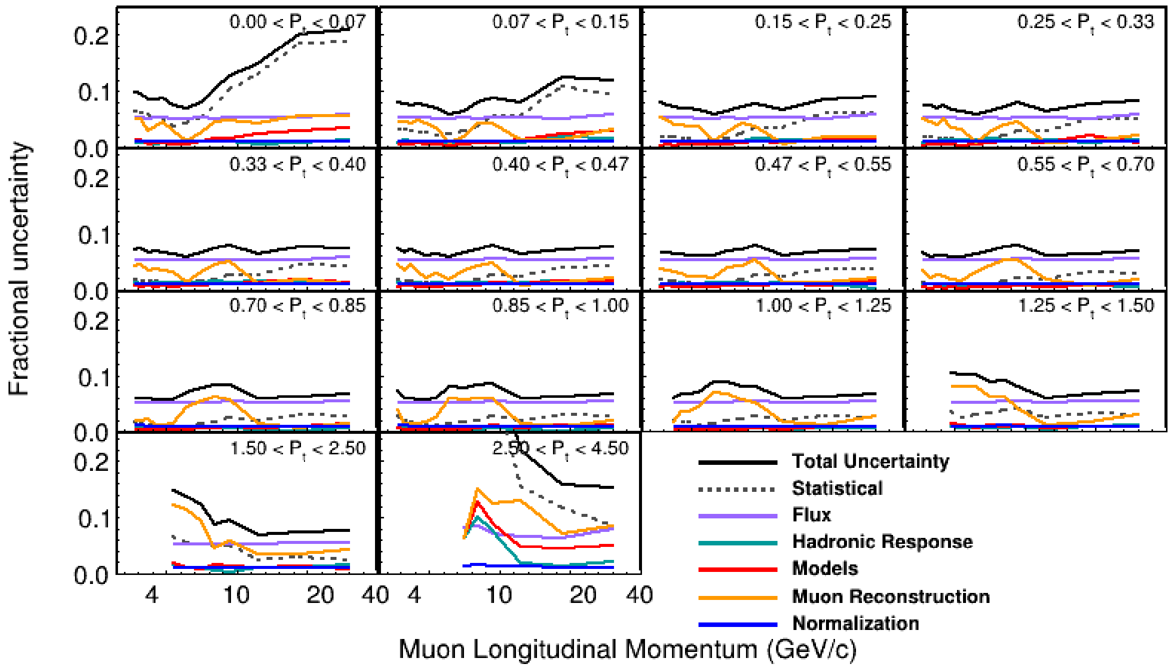

FIG. 19. antineutrinos cross section uncertainty breakdown

.

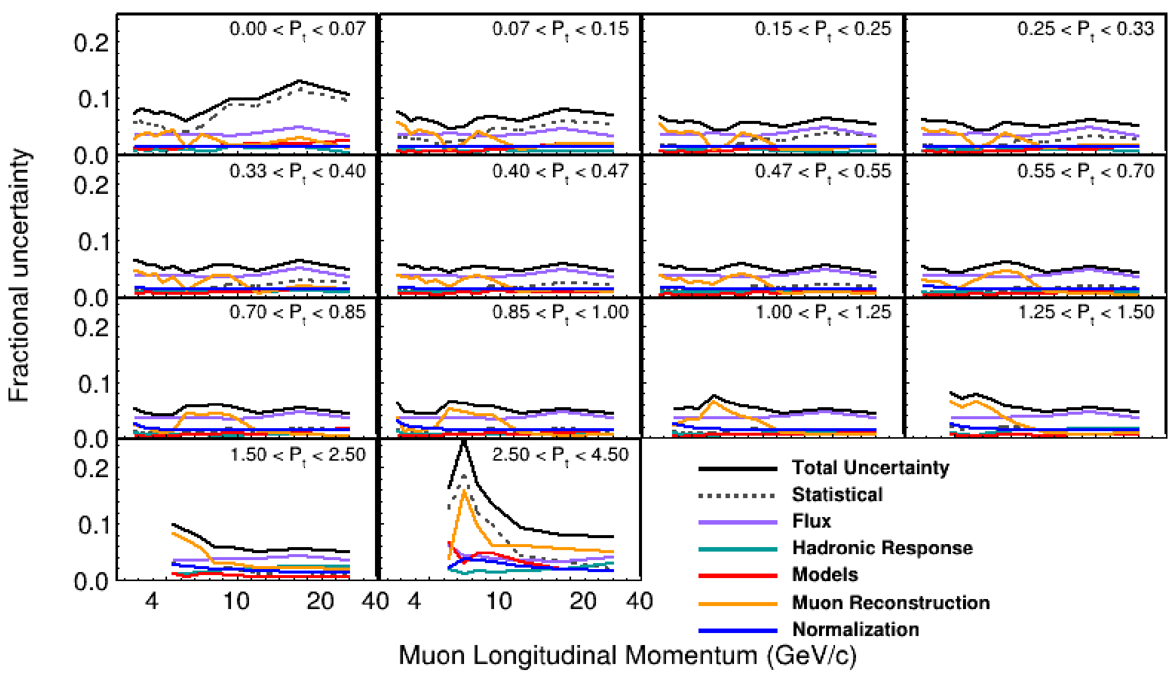

FIG. 20. Neutrino cross section uncertainty breakdown

.

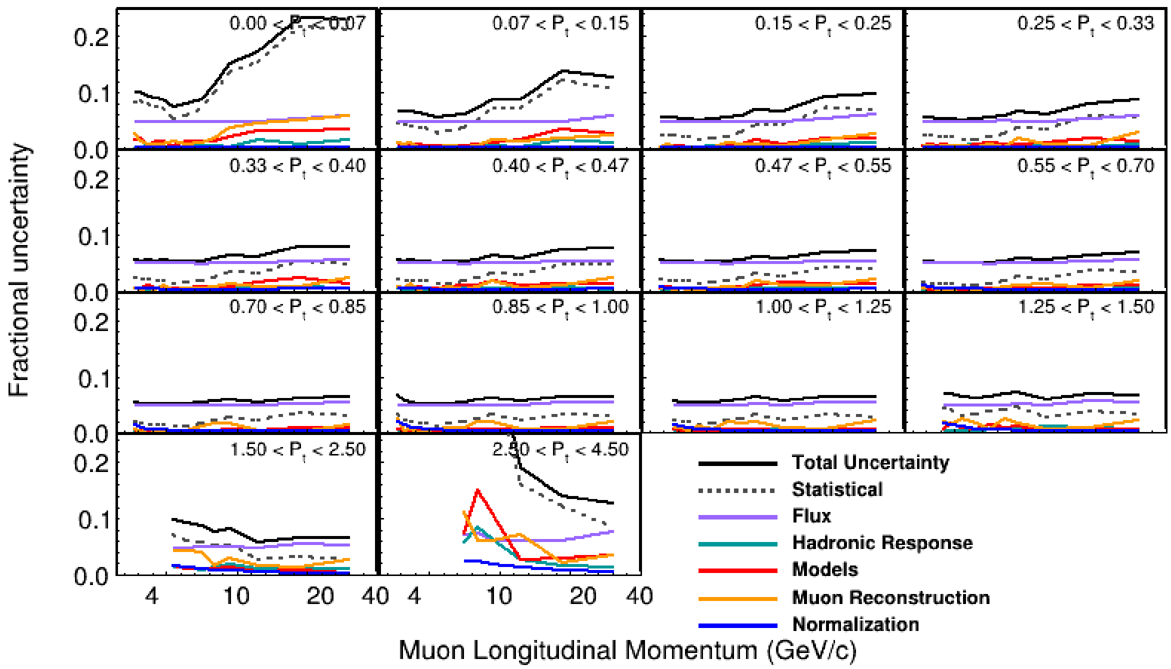

FIG. 21. Unweighted neutrino to antineutrinos cross section ratio uncertainty breakdown.

.

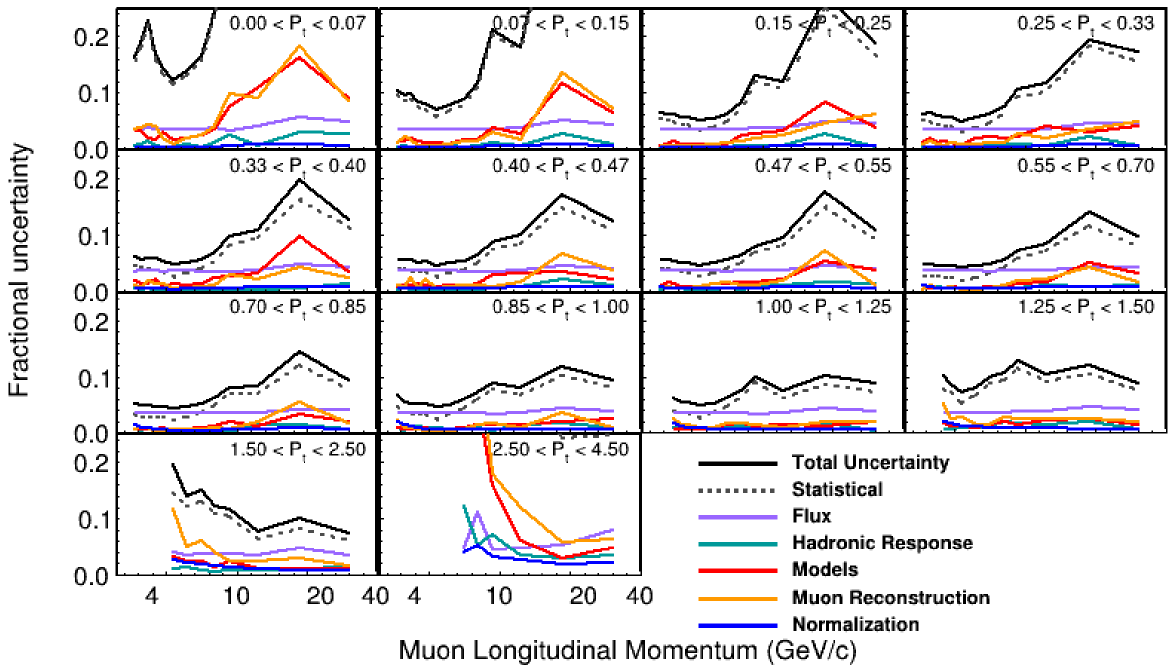

FIG. 22. Reweighted neutrino to antineutrinos cross section ratio (prior to some normalizations) uncertainty breakdown.

.

VIII. RESULTS

A. Cross Section Extraction

The cross section measurement that is extracted depends on the incoming flux since it was extracted in terms of muon kinematics. An absolute cross section measurement in terms of neutrino energy would be independent of the incoming flux. The corresponding neutrino cross section measurement (ie. inclusive double differential cross section measurement on hydrocarbon in terms of muon kinematics) was extracted in the Low Energy era when the flux peaked at 3 GeV, instead of the 6 GeV for the Medium Energy era. (The flux for the Medium Energy era was used for this measurement and is shown in FIG. 3). The corresponding Low Energy era measurement is in [43]. The same neutrino cross section measurement was then extracted in the Medium Energy era and is in [37]. The Medium Energy era neutrino measurement has been re-extracted for this analysis, with the newer flux constraint [25].

The unfolded efficiency corrected event distributions are normalized by the flux, bin width, and number of targets to extract the cross sections. The energy transferred from the incoming neutrino dictates the probability of it to participate in a particular type of neutrino nucleus interaction. This is an inclusive analysis and hence, all charged current interactions are considered signal. The different interaction types are Quasi elastic (QE) in which there is an outgoing nucleon and muon, resonant pion production (Resonant) in which a resonance gets created which then decays to a pion and a nucleon, and deep inelastic scattering (DIS) which happens at the quark level and produces a lot of hadronic activity. 2p2h is a multinucleon effect in which two particles get knocked out of the nucleus as a result of the incoming neutrino. The simulated amounts of each type of interaction are shown on the cross section plots.

The antineutrinos cross section in antineutrinos mode is shown in FIG. 23. The neutrino cross section in neutrino mode is shown in FIG. 24. It is useful to take ratios to the prediction and those are shown in FIG. 25 and FIG. 26. The plots also show which interaction channels dominate in which parts of phase space. For example, higher muon longitudinal and transverse momenta are required for Deep Inelastic Scattering. Furthermore, the ratio plot demonstrates that the models need improvement as the model prediction doesn't agree with the data.

The two cross section measurements were combined in the form of an unweighted cross section ratio shown in FIG. 27 and FIG. 28.

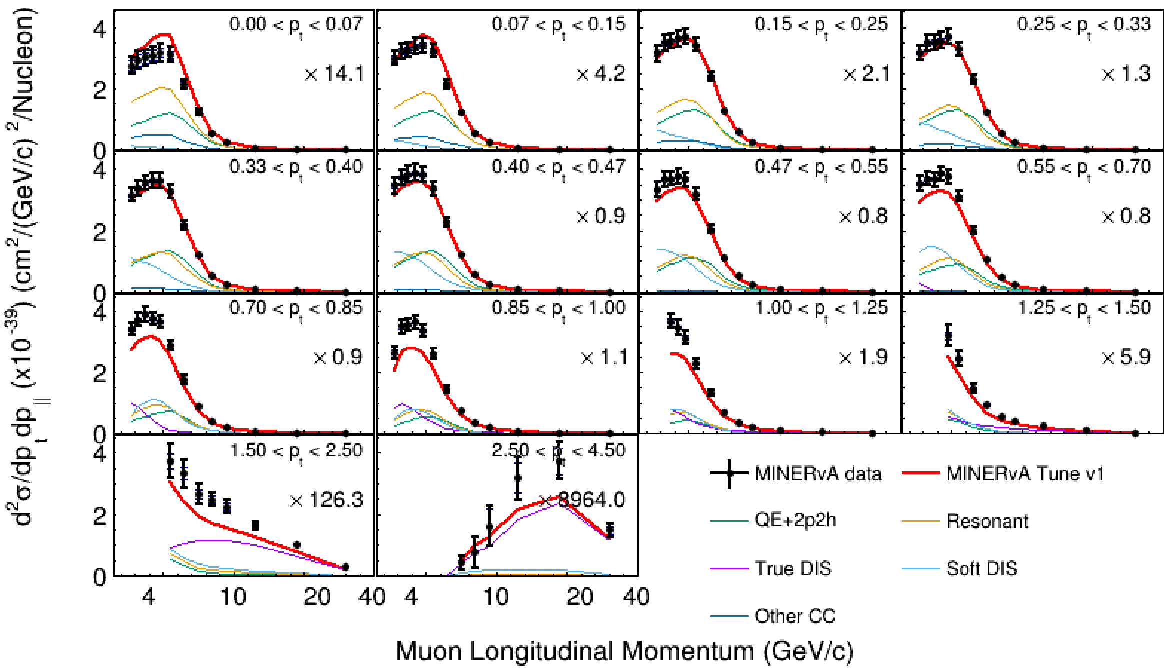

FIG. 23. Cross section for antineutrinos in the antineutrino-enhanced beam as a function of muon kinematics, along with the prediction from the simulation tuned on an independent data set. The predicted contributions from different processes, as described in the text, are also shown.

.

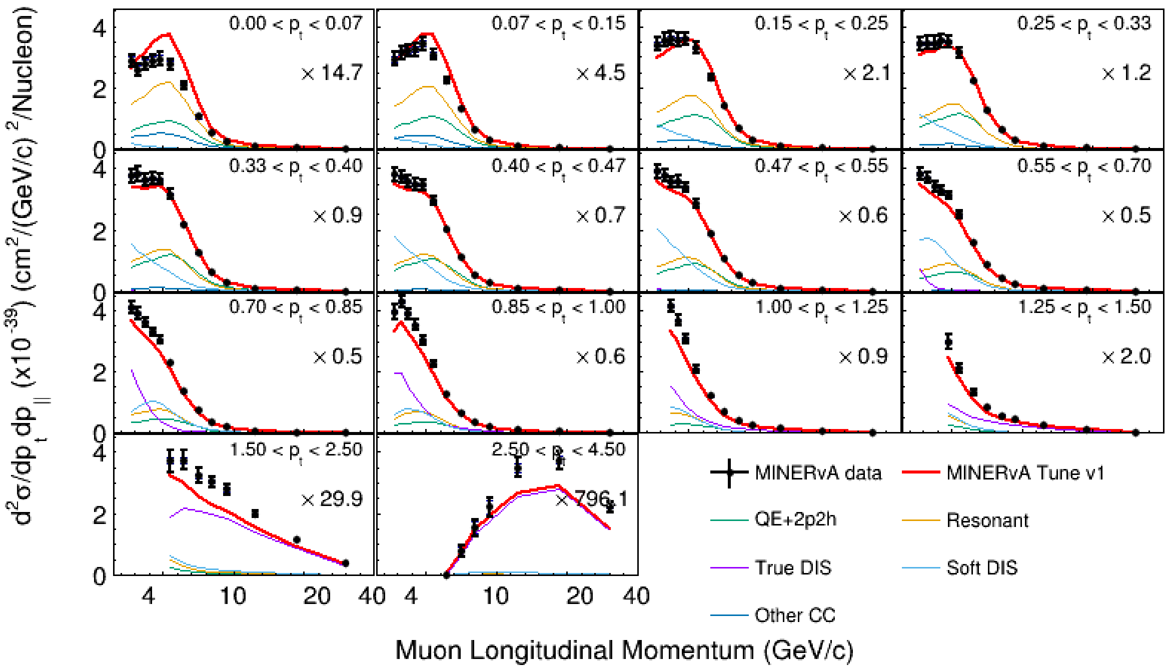

FIG. 24. Cross section for neutrinos in the neutrino-enhanced beam as a function of muon kinematics, along with the prediction from the simulation tuned on an independent data set. The predicted contributions from different processes, as described in the text, are also shown.

.

In the Models section, comparisons are done between this unweighted extracted cross section ratio and several other models. The shortcomings of this ratio result are that it is difficult to interpret since the incoming neutrino and antineutrinos fluxes are different.

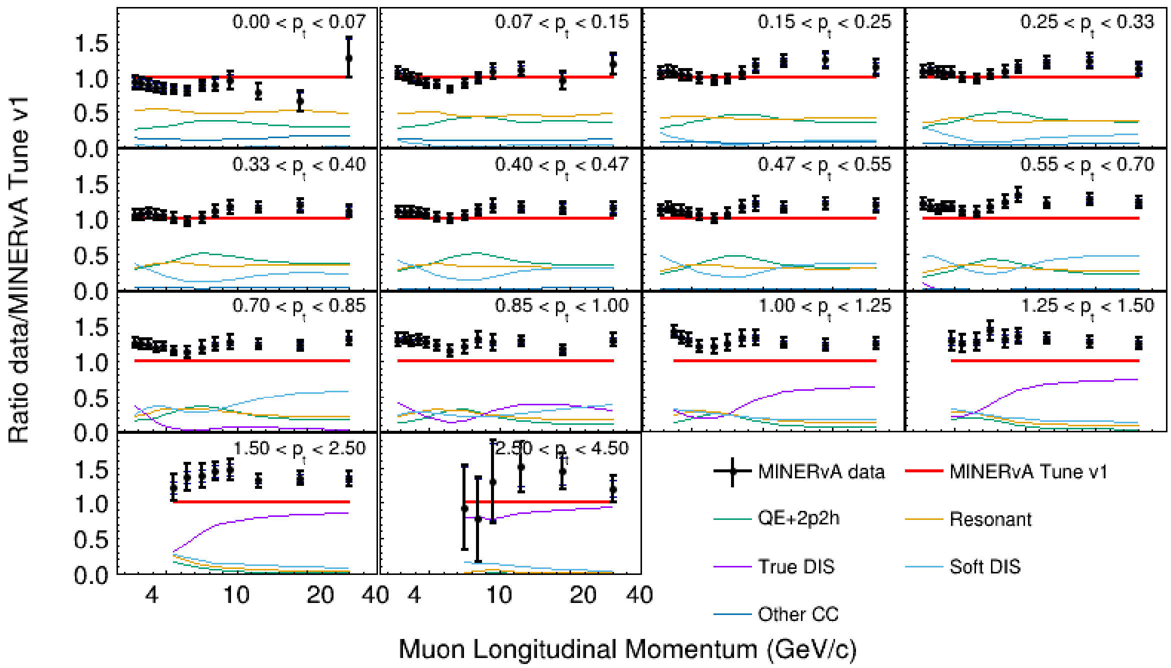

FIG. 25. The ratio of the antineutrino cross section in antineutrino-enhanced beam to the default MINERvA simulation as a function of muon kinematics, with the predicted contributions.

.

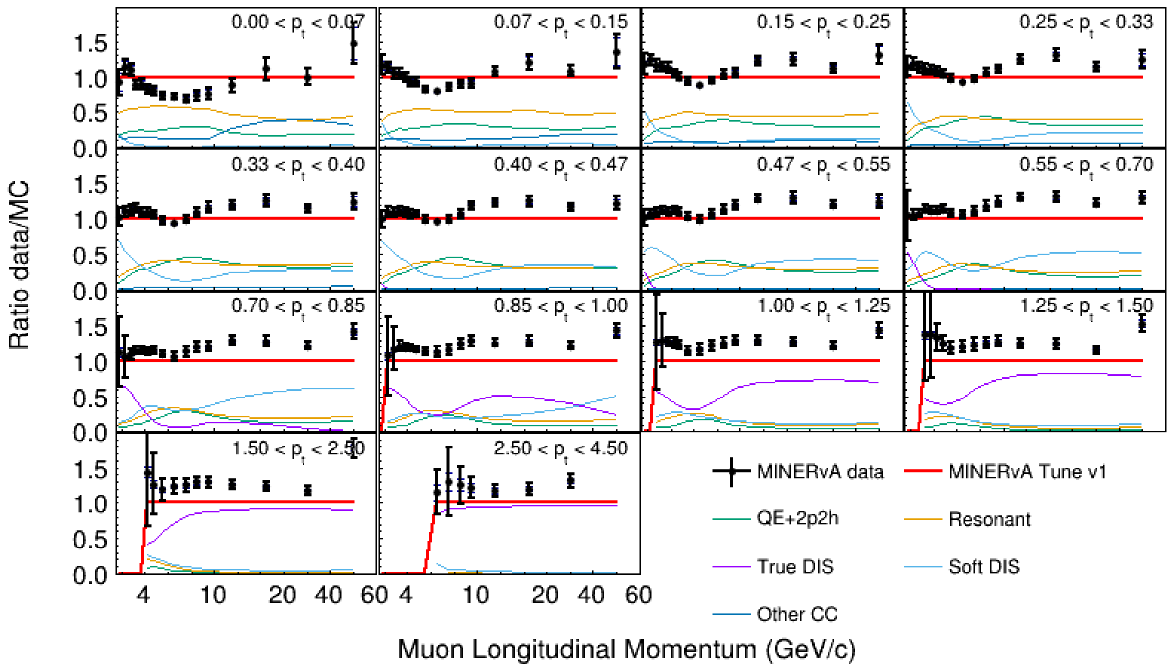

FIG. 26. The ratio of the neutrino cross section in neutrino-enhanced beam to the default MINERvA simulation as a function of muon kinematics, with the predicted contributions.

.

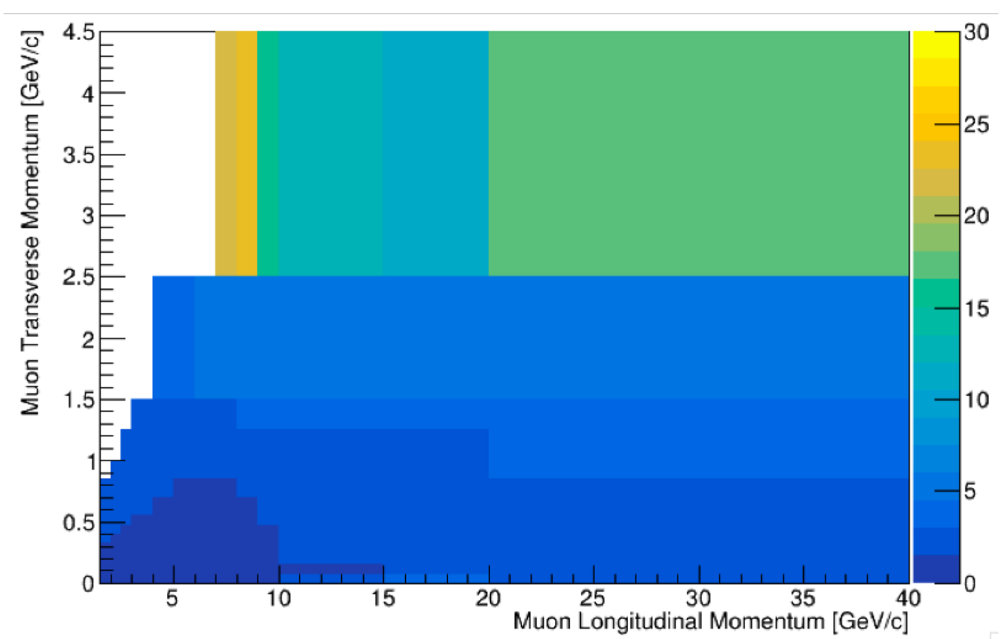

FIG. 27. Neutrino to antineutrinos unweighted cross section ratio

.

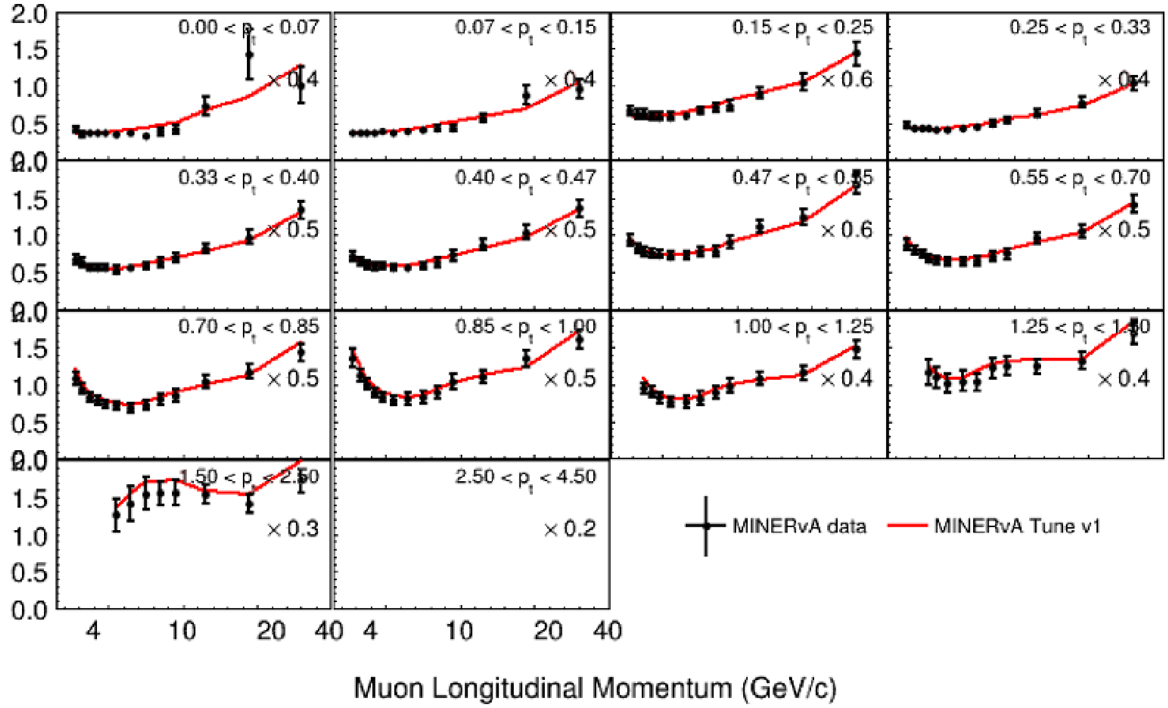

FIG. 28. Neutrino to antineutrinos unweighted cross section ratio with the total uncertainty on the extracted cross section ratio.

.

B. Rose Petal Reweighting Technique

This subsection will describe how the neutrino flux in neutrino mode does not match the antineutrinos flux in antineutrinos mode, as in FIG. 3, and will elaborate on the technique used to reduce the difference between the fluxes in both modes.

From FIG. 3, it is apparent that the neutrino flux in neutrino mode per POT is overall higher than the antineutrinos flux in antineutrinos mode per POT. At energies lower than the Medium Energy (ME) flux peak of 6 GeV, the fluxes per POT seem to be closer to each other. However, at energies higher than that of the focusing peak, the antineutrinos flux in antineutrinos mode seems to fall more steeply than the neutrino flux in neutrino mode. Therefore, there are more high energy neutrinos in neutrino mode than high energy antineutrinoss in antineutrinos mode. For this reason, when trying to reweight the neutrino flux to match the antineutrinos flux, the higher energy neutrino tail will need to be weighted down in order to match the lower level of the antineutrinos high energy flux tail. Furthermore, it is interesting to note that the neutrino contamination in antineutrinos mode at high neutrino energies equals the antineutrinos flux in antineutrinos mode. This will drive the motivation for having a fourth sample comprised of the neutrino flux in antineutrinos mode, to use in the reweighting of the neutrino flux in neutrino mode to match the antineutrinos flux in antineutrinos mode.

The ratio of the neutrino flux to antineutrinos flux is shown in FIG. 29. Since this ratio is not consistent with 1, it makes it difficult, to interpret the result of taking the neutrino to antineutrinos cross section ratio. This is because the goal of taking the cross section ratio is to better understand differences between the two modes which are by virtue of what is inherently different in both modes. However, having a different flux in the numerator and the denominator, complicates matters because now the ratio's inconsistency with 1 is not purely due to the difference in both the modes, but also because of a difference in fluxes. For instance, the ratio of the neutrino cross section extracted in the neutrino beam to the same neutrino cross section extracted on neutrinos in the antineutrinos beam is not consistent with 1, due to the fluxes being different. This example illustrates the need to get the fluxes to match in the numerator and the denominator when taking cross section ratios. Neutrino oscillation experiments are interested in understanding whether neutrinos and antineutrinoss oscillate differently and so, taking meaningful neutrino to antineutrinos cross section ratios is useful.

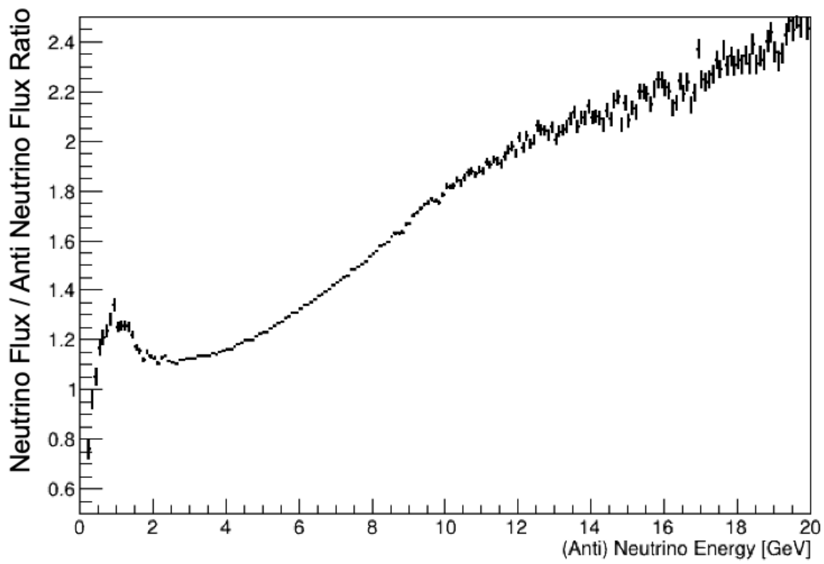

FIG. 29. The ratio of the neutrino flux in the neutrino enhanced beam to the antineutrinos flux in the antineutrinos enhanced beam.

.

In order to go from a difficult to comprehend unweighted neutrino to antineutrinos cross section ratio, to a meaningful cross section ratio, it was decided to reweight the neutrino flux in neutrino mode to match the antineutrinos flux in antineutrinos mode. For this reweighting technique, the neutrino flux in neutrino mode was broken up into different rings and then a linear combination of those rings was sought out which would be equivalent to the antineutrinos flux. Hence, some rings would be weighted up and some rings would be weighted down in order to achieve the antineutrinos flux. Then, the cross section would be extracted in each hexagonal ring and stitched together using the coefficients from the reweighted neutrino flux linear combination to arrive at a reweighted neutrino cross section extracted on a flux which matches that of the antineutrinos cross section.

Several variations of this study were done using 6 rings, 8 rings, 12 rings, 3 rings, and 12 triangles. The technique used is referred to as the rose petal reweighting technique due to the nature of rose petals being more closely bound to the stem in the centre of the rose and less tightly bound away from the centre of the rose. Similarly, the highest neutrino flux is in the most forward going direction of the beam and begins to fall off at larger angles from the beam centre. Furthermore, rose petals circle around the stem, and so the shape of the rose petal is close to the shape of the rings used for this study, as opposed to the shape of daisy petals for example.

The result of using 12 hexagonal rings in neutrino mode to reweight the neutrino flux to match the antineutrinos flux is shown in FIG. 30. It can be seen that the reweighted neutrino to antineutrinos flux ratio, though an improvement from the unweighted ratio in FIG. 29 is still not consistent with 1. At low neutrino energies, the ratio is close to 1 but at high neutrino energy, the ratio grows rapidly.

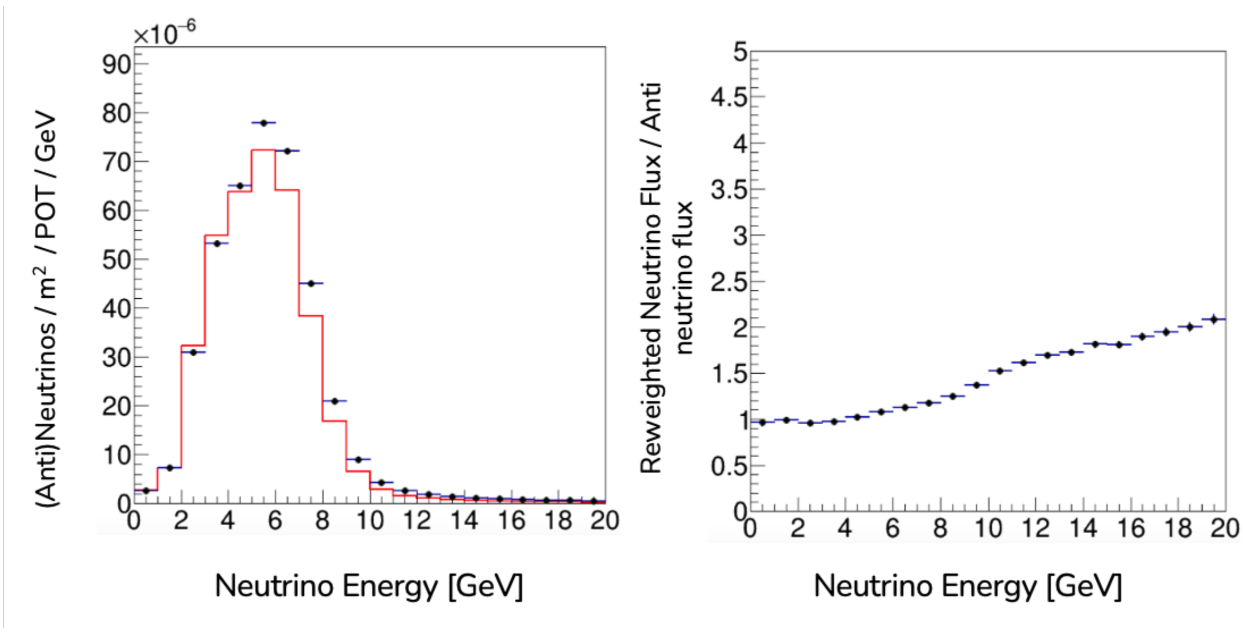

FIG. 30. [Left] The red curve is the antineutrinos flux and the data points are the reweighted neutrino flux. The neutrino flux was reweighted using 12 rings of the neutrino flux in neutrino mode. [Right] The ratio of the reweighted neutrino flux to the antineutrinos flux.

In order to tame the reweighted neutrino to antineutrinos flux ratio at high neutrino energies, an additional hexagonal ring was added which comprised of the neutrino flux in antineutrinos mode. One way in which neutrinos end up in the antineutrinos beam is through the decay of pions that go through the neck of the horns and don't get focused. These pions are the most forward going and so have high energies, consequently creating neutrinos in the antineutrinos beam with high energies. Therefore, as can be seen in FIG. 31 a) the blue curve shows the contribution from neutrinos in the antineutrinos beam.

The study done with 12 rings was repeated with the additional hexagonal ring of neutrinos in antineutrinos mode, for a total of 13 rings. After reweighting with the set of 13 rings, the reweighted neutrino to antineutrinos flux looks like FIG 32 [Left]. This is still not a ratio of 1, it tames the growing high energy tail of the ratio, but at the cost of a poorer fit between reweighted neutrino and antineutrinos fluxes at lower neutrino energies.

In order to extract a reweighted neutrino cross section, we sought to extract the cross section in each ring and then combine it using the weights that were used for reweighting the neutrino flux. However, the unfolding step was not successful for some of the 13 rings and therefore, the study was repeated with 4 rings, ie 3 rings in neutrino mode and 1 ring of neutrinos in antineutrinos mode. Using 4 rings, we were able to retrieve the same ratio result that we saw using 13 rings. This is shown in FIG. 32.

It is interesting to note the weights that were used to achieve the ratio in FIG. 32. Ring 1 corresponds to the inner most hexagonal ring, Ring 2 is the middle ring, and Ring 3 is the outer ring. Of the 4 rings, 3 rings were weighted down and one ring (ie Ring 3) was weighted up by a factor of 4. This seems intuitive looking at the fluxes for each ring plotted out in FIG. 31 a) and the ratios of the fluxes of Ring 2 and Ring 3 to Ring 1 shown in FIG. 31 b). This weighting seems intuitive because the flux in Ring 3 looks the closest to the antineutrinos flux in antineutrinos mode since it's also falling steeply at higher energies and has a higher flux slightly below the focusing peak. Therefore, it makes sense to weight it up and then weight down the fluxes in the other rings. It is especially useful to weight down Ring 4 since that includes a sample of high energy neutrinos. Despite this reweighting, the neutrino flux doesn't match the antineutrinos flux perfectly, but matches it better than the unweighted neutrino to antineutrinos flux ratio. FIG. 33 predicts how much the neutrino cross section would change if extracted with a flux that matched the antineutrinos flux exactly, in the monte carlo.

The reweighting technique is currently being developed and will be completed soon. Reweighting the neutrino flux to match the antineutrinos flux is useful for computing the neutrino to antineutrinos cross section ratio, since if the fluxes match exactly, the differences in that ratio will be because of the different modes and not due to a difference in incident flux.

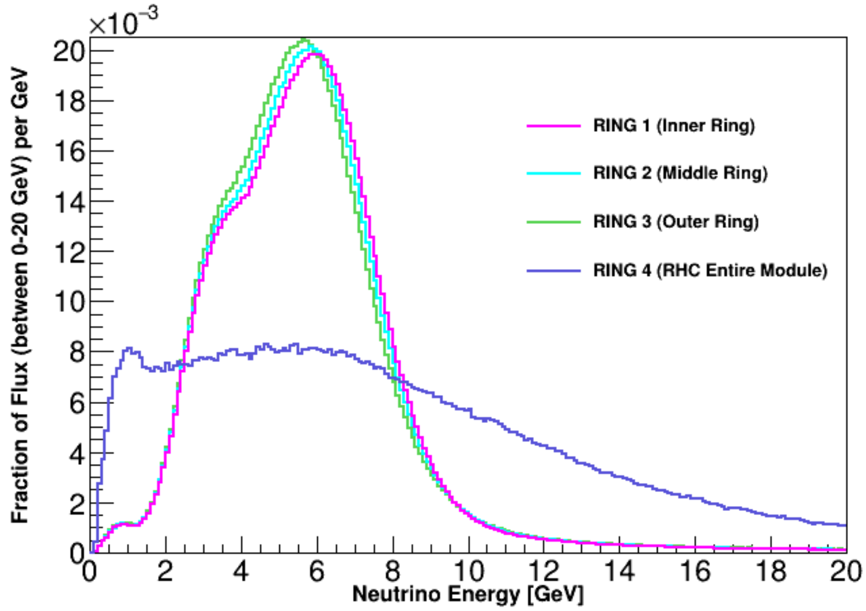

(a)

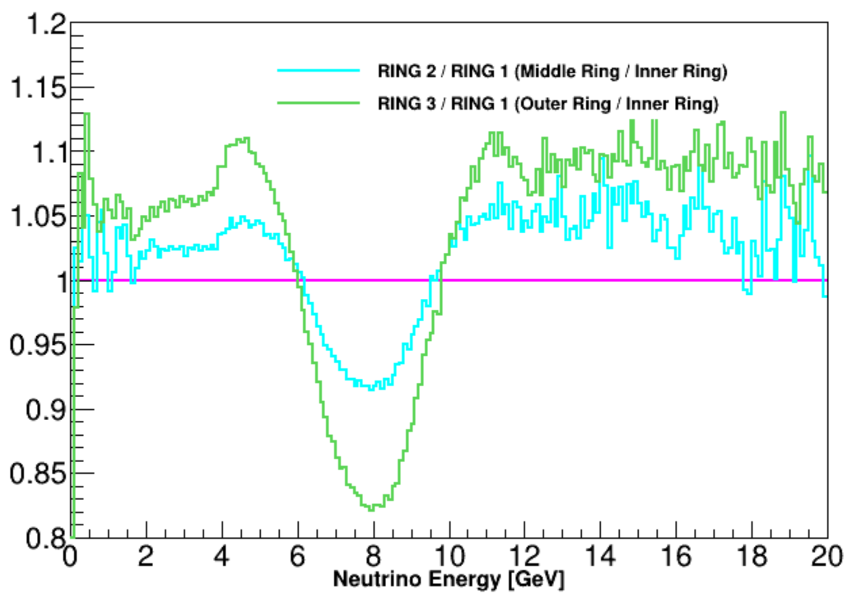

(b)

FIG. 31. [TOP] a) The fluxes in each ring of neutrinos. Ring 1 corresponds to the inner most hexagonal ring, Ring 2 the middle ring, and Ring 3 the outermost ring, all in the neutrino enhanced beam. Ring 4 represents the neutrinos in the antineutrinos enhanced beam. [BOTTOM] b) The ratio of Ring 2 to Ring 1 and Ring 3 to Ring 1.

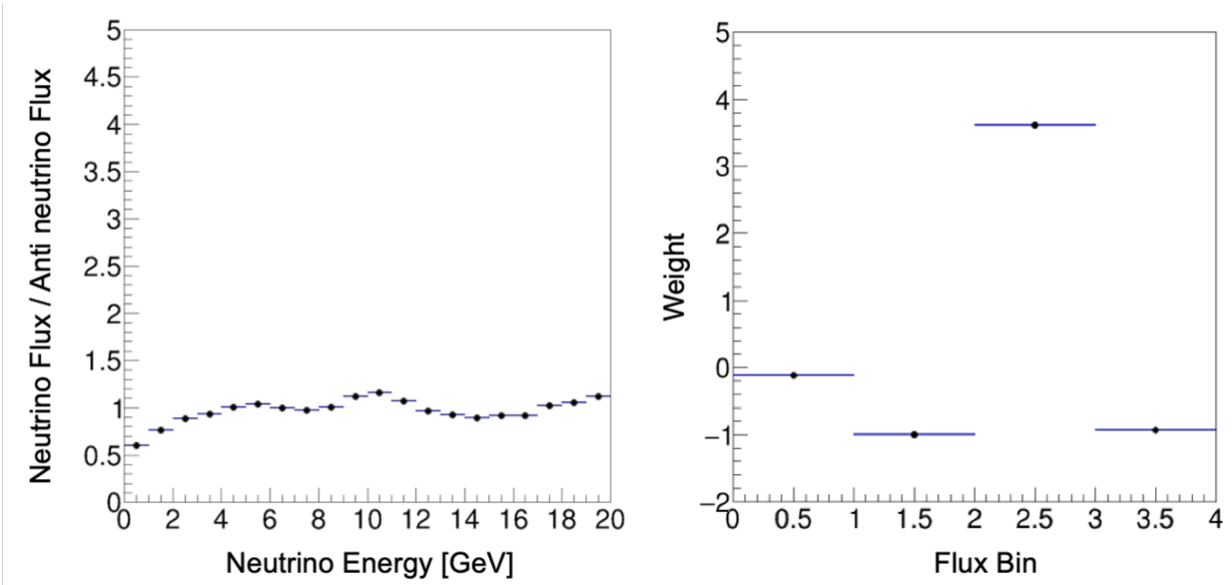

FIG. 32. [Left] The reweighted neutrino to antineutrinos flux ratio, computed using 4 rings for reweighting the neutrino flux. [Right] The weights required for each of the 4 rings to achieve the reweighted neutrino to antineutrinos flux ratio on the left.

IX. MODEL COMPARISONS

There are several different neutrino interaction generators that are in use in the neutrino community. NEUT is used by the Tokai to Kamiokande (T2K) experiment in Japan, while GENIE is used in Fermilab-based neutrino experiments like MINERvA, and the short baseline program. Within those generators, there is a choice of different models for different sub-processes.

The nucleus is comprised of nucleons and to understand neutrino nucleus interactions, it is important to model the nucleus. The simplest initial state model used is the Fermi Gas Model (FG) which treats the nucleons as non interacting with each other and free to move inside the nucleus. Nucleons obey the Pauli Exclusion principle. The Fermi energy is the energy of the highest occupied state and the binding energy is the energy that is needed to remove a nucleon from the nucleus.

The Local Fermi Gas Model (LFG) is a model which accounts for the spherically symmetric density of the nucleons and the Fermi momentum being dependent on the distance from the centre of the nucleus. There is also the Spectral Function (SF) model of the initial state which accounts for short range correlations in the nucleus. Short range correlations were

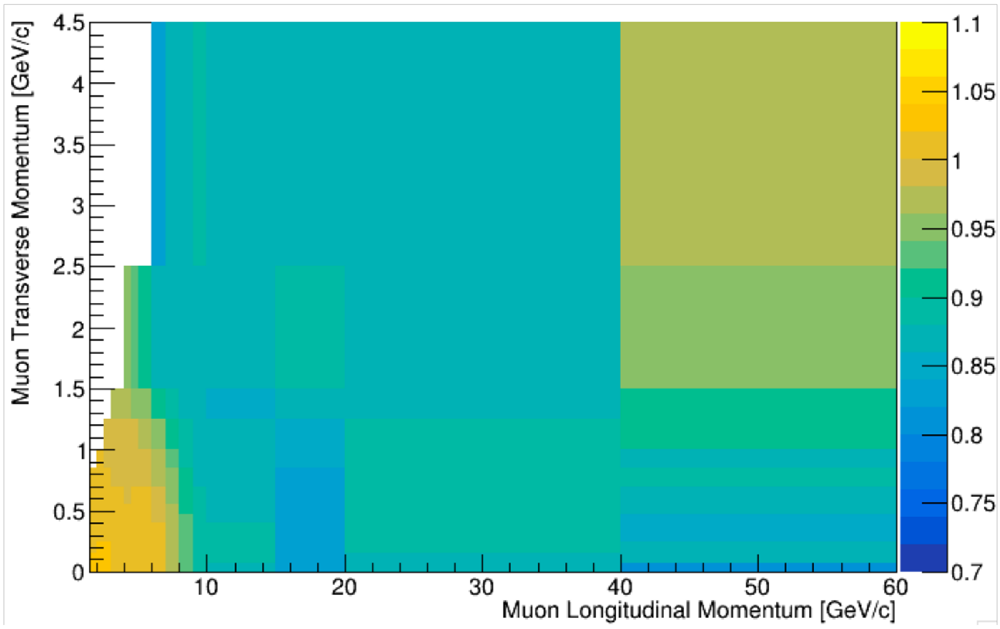

FIG. 33. Ratio: Neutrino cross section using neutrino flux / Neutrino cross section using neutrino flux matched to antineutrinos flux.

.

observed in electron scattering experiments in which a correlated partner nucleon also got knocked out in addition to the struck nucleon. Hence, short range correlated pairs are two close nucleons which have high relative momentum and low centre of mass momentum. The nuclear spectral function is available for specific nuclei including helium, carbon, and oxygen. Therefore, each of the different models predict a different distribution for the nucleon's momentum distribution, as seen in FIG. 34.

Neutrino interactions that happen in the nucleus produce particles, but these particles can only be visible to us once they exit the nucleus. However, on their way out of the nucleus, the particles can continue to interact and this is referred to as final state interactions (FSI). Final state interactions are complex elastic/inelastic scattering off other nucleons in which hadrons can get absorbed or produced. The intranuclear cascade model, understood to be the "billiard balls" model is used to model FSI. It treats particles as classically moving along a straight line with some probability of interacting. The hN intranuke model considers many possible interactions and computes the cross section for each process until all the particles leave the nucleus. Hence, a cascade of hadronic interactions is calculated. The hA intranuke model uses a different approach of considering just one "effective" interaction and is tuned to hadron-nucleus data. Hence, the key differences between the hA and hN models appear after the final state interaction is chosen, in that the hA model is heavily based on data to model it as a single interaction, whereas the hN model uses a cascade approach of multiple interactions. Both models use the same mean free path values but use a different pion nucleon cross section [44] [45].

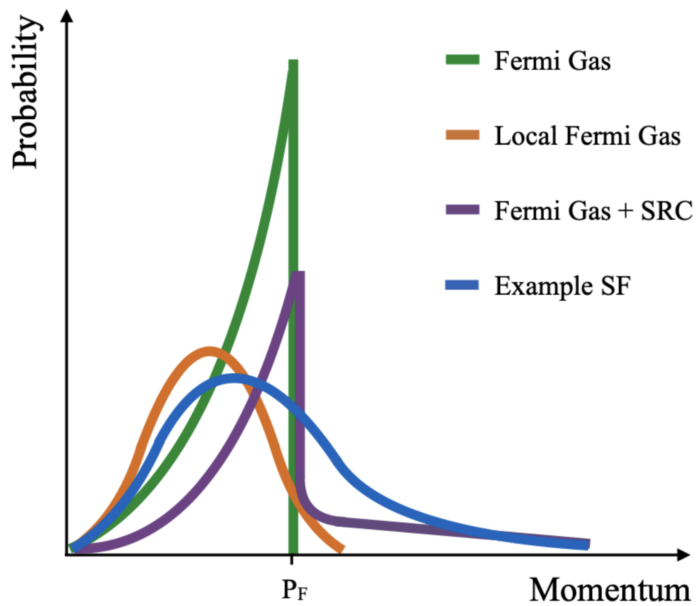

FIG. 34. Predicted nucleon momentum distribution in the initial state from various different models [2].

.

Model comparisons were done for different models (FIG. 35 and FIG. 36) for the unweighted neutrino to antineutrinos cross section ratio. They are shown below.

The NEUT Spectral Function (SF) model appears to do a better job of describing the data than NEUT Local Fermi Gas (LFG). All of the GENIE model predictions appear to be close to each other and better than the NEUT predictions. Furthermore, the MINERvA Tune v1 seems to describe the data the best among the model predictions, though it too requires improvement as the chi squared value is 705.6 with 192 degrees of freedom for the cross section ratio.

The models do a much better job of capturing the ratio of neutrino to antineutrinos cross sections than they do of capturing either of the individual cross sections, as is evident from

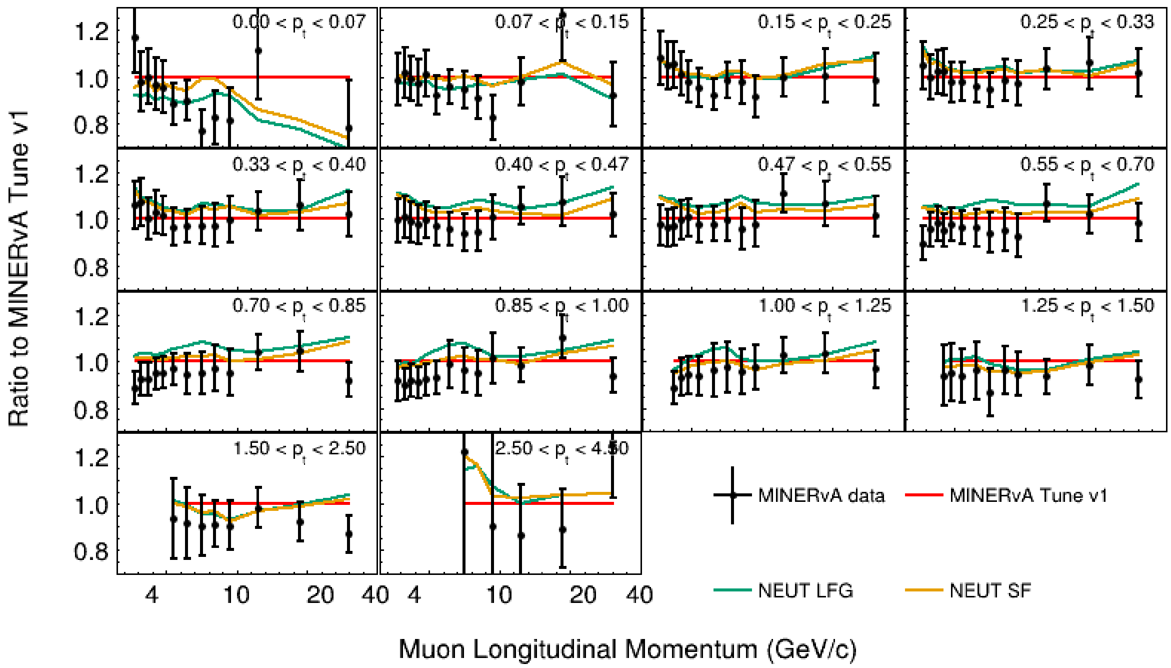

FIG. 35. NEUT ratio model comparisons for the unweighted neutrino to antineutrinos cross section ratio.

.

FIG. 37 and FIG. 38. This is a work in progress and more model comparisons are currently being worked on.

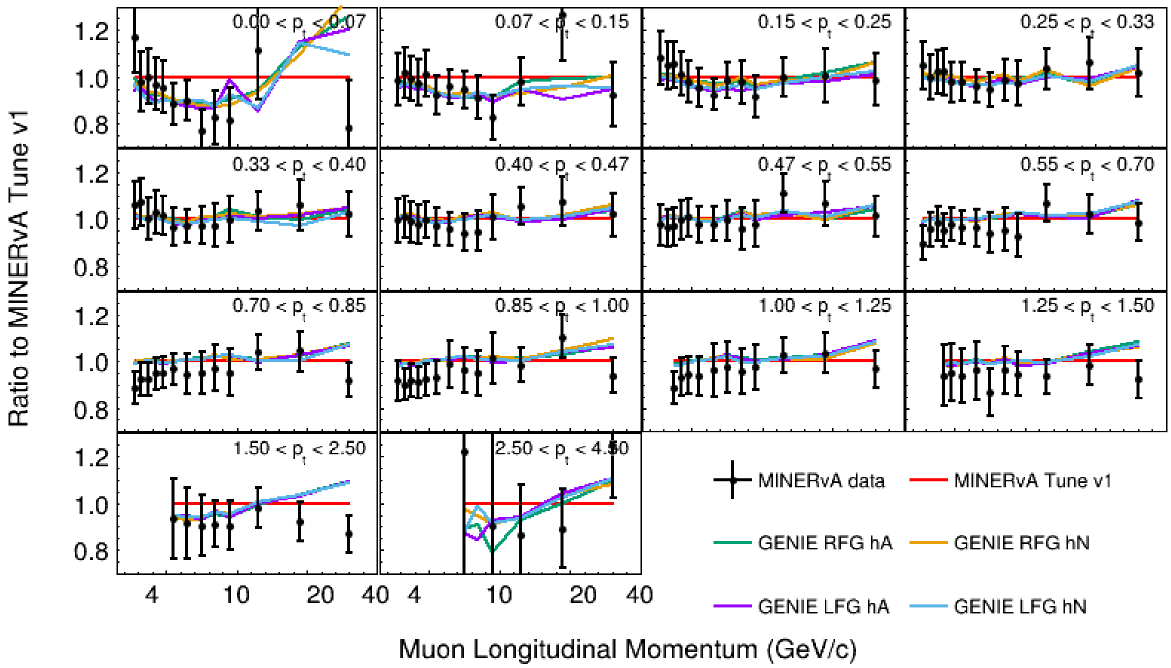

FIG. 36. GENIE v3 ratio model comparisons for the unweighted neutrino to antineutrinos cross section ratio.

.

Process Variant	χ^2 **for ratio**	χ^2 **for antineutrinos mode**
MINERvA Tune v1	705.6	2734.7
GENIE RFG hA	1400.8	1965.2
GENIE RFG hN	1392.5	1972.1
GENIE LFG hA	1364.8	2206.8
GENIE LFG hN	1358.4	2187.8
NEUT LFG	2434.3	5835.8
NEUT SF	1418.6	6355.4

TABLE I. The chi2 computed for the various model predictions for the unweighted neutrino to antineutrinos cross section ratio in the second column. The chi2 for antineutrinos mode in the third column, DOF = 192.

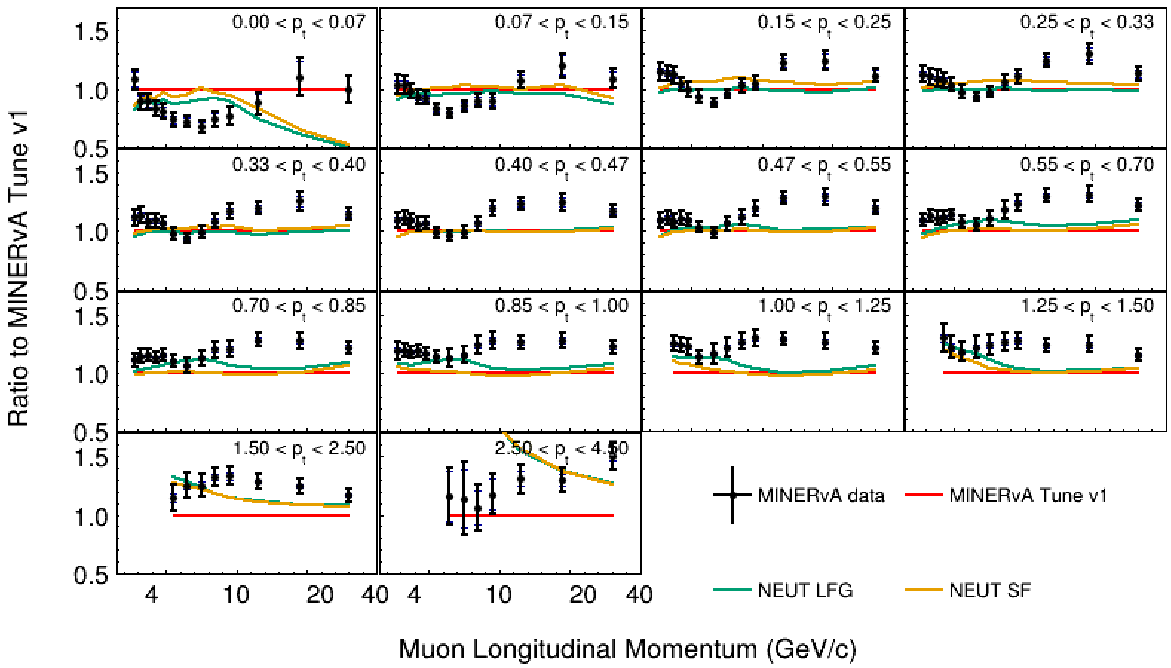

FIG. 37. NEUT model comparisons for the neutrino cross section extracted in the neutrino enhanced beam.

.

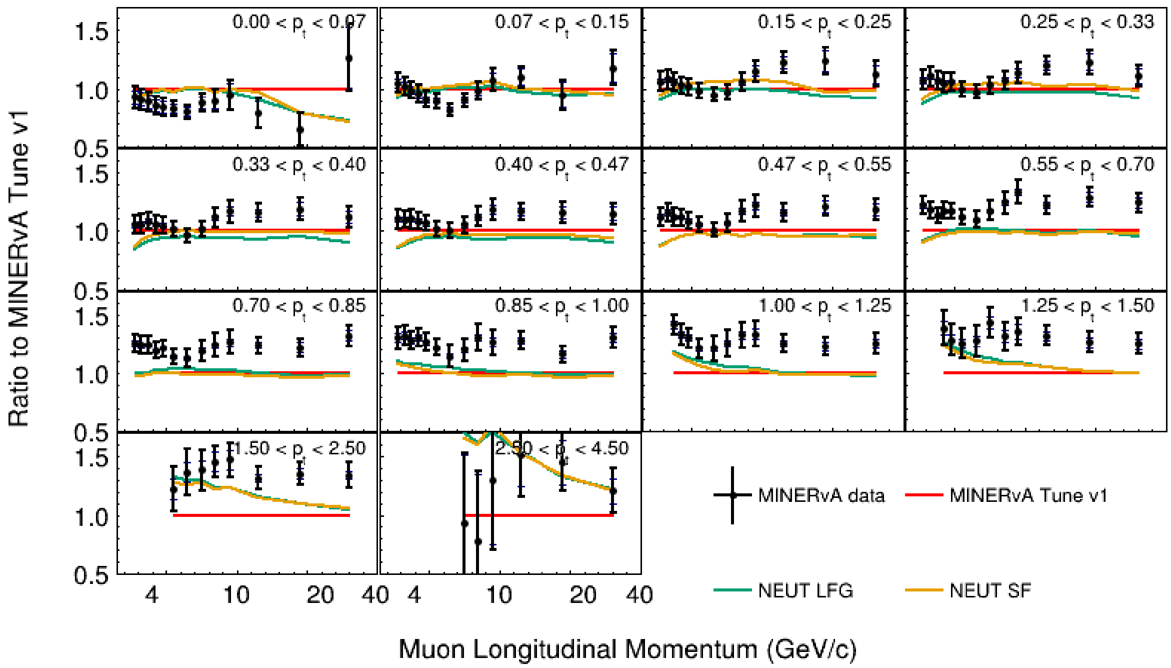

FIG. 38. NEUT model comparisons for the antineutrinos cross section extracted in the antineutrinos enhanced beam.

.

X. CONCLUSION

In conclusion, the double differential inclusive antineutrino cross section measurement on hydrocarbon was extracted in terms of muon kinematics. The same measurement was extracted in neutrino mode using the newer flux constraint and the ratio was taken. The models do a better job of predicting the ratio than they do of capturing the neutrino or antineutrinos cross sections individually. The MINERvA model tuned on the Low Energy (LE) era, MINERvA Tune v1, is better at predicting the cross section ratio, than the other models analyzed.

This is a useful measurement because it doesn't require hadronic energy reconstruction and instead uses variables which are proxies for neutrino energy and the four momentum squared transferred to the nucleus. This measurement provides a useful benchmark for improving cross section models for use in neutrino oscillation experiments.

XI. SPECIFIC ROLE FOR MSC PROJECT

My specific role for this MSc project was extracting this particular measurement: Double differential antineutrino cross section on CH in terms of muon kinematics and ratio to neutrino cross section. I have also participated in the data preservation effort and worked on a paper review [46].

[1] M. Sajjad Athar and S. K. Singh, Neutrinos and their interactions, Eur. Phys. J. ST **230**, 4215 (2021), arXiv:2111.12328 [hep-ph].

[2] A. Ashkenazi, Neutrino cross sections and interactions, `https://npc.fnal.gov/wp-content/uploads/2021/07/210624_nuInteractionsCrossSections.pdf`.

[3] P. Adamson *et al.*, The NuMI Neutrino Beam, Nucl. Instrum. Meth. A **806**, 279 (2016), arXiv:1507.06690 [physics.acc-ph].

[4] B. Messerly, *Single Charged Pion Production by Muon Neutrinos in the MINERvA Detector Using the NuMI Beam*, Ph.D. thesis, Pittsburgh U. (2019).

[5] L. Aliaga *et al.* (MINERvA), Design, Calibration, and Performance of the MINERvA Detector, Nucl. Instrum. Meth. A **743**, 130 (2014), arXiv:1305.5199 [physics.ins-det].

[6] P. Adamson *et al.* (MINOS), Neutrino and Antineutrino Inclusive Charged-current Cross Section Measurements with the MINOS Near Detector, Phys. Rev. D **81**, 072002 (2010), arXiv:0910.2201 [hep-ex].

[7] C. Patrick, A place for minerva, `https://minerva-docdb.fnal.gov/cgi-bin/sso/RetrieveFile?docid=6421&filename=inss_place_patrick.pdf&version=4`.

[8] T. Toshito (Super-Kamiokande), Super-Kamiokande atmospheric neutrino results, in *36th Rencontres de Moriond on Electroweak Interactions and Unified Theories* (2001) arXiv:hep-ex/0105023.

[9] J. Wolcott (NOvA), Impact of cross section uncertainties on NOvA oscillation analyses, PoS **NuFACT2018**, 098 (2019), arXiv:1812.05653 [hep-ex].

[10] J. Kleykamp, *A-scaling of CCQE-like cross sections at MINERvA*, Ph.D. thesis, Rochester U., Rochester U. (2021).

[11] K. S. McFarland, Neutrino Interactions, in *61st Scottish Universities Summer School in Physics: Neutrinos in Particle Physics, Astrophysics and Cosmology (SUSSP61)* (2008) pp. 65–90, arXiv:0804.3899 [hep-ex].

[12] M. Goodman, The deep underground neutrino experiment, Advances in High Energy Physics **2015**, 1 (2015).

[13] D. G. Michael *et al.* (MINOS), The Magnetized steel and scintillator calorimeters of the MINOS experiment, Nucl. Instrum. Meth. A **596**, 190 (2008), arXiv:0805.3170 [physics.ins-

det].

[14] L. Ren, *Measurement of Neutrino and Antineutrino Total Charged-Current Cross Sections on Carbon with MINERvA*, Ph.D. thesis, U. Pittsburgh (main) (2017).

[15] T. P. D. Group, Pdg summary tables, `https://pdg.lbl.gov/2020/listings/rpp2020-list-muon.pdf`.

[16] M. Bardon, P. Norton, J. Peoples, A. M. Sachs, and J. Lee-Franzini, Measurement of the momentum spectrum of positrons from muon decay, Phys. Rev. Lett. **14**, 449 (1965).

[17] C. Patrick, *Measurement of the Antineutrino Double-Differential Charged-Current Quasi-Elastic Scattering Cross Section at MINERvA*, Ph.D. thesis, Northwestern U. (2016).

[18] R. Fruhwirth, Application of Kalman filtering to track and vertex fitting, Nucl. Instrum. Meth. A **262**, 444 (1987).

[19] R. Luchsinger and C. Grab, Vertex reconstruction by means of the method of Kalman filter, Comput. Phys. Commun. **76**, 263 (1993).

[20] A. Bercellie (MINERvA), *Muon neutrino charged current single pion production on various targets in the MINERvA detector*, Ph.D. thesis, Rochester U., Rochester U. (2022).

[21] N. Tagg *et al.* (MINERvA), Arachne - A web-based event viewer for MINERvA, Nucl. Instrum. Meth. A **676**, 44 (2012), arXiv:1111.5315 [hep-ex].

[22] S. Agostinelli *et al.* (GEANT4), GEANT4–a simulation toolkit, Nucl. Instrum. Meth. A **506**, 250 (2003).

[23] C. Alt *et al.* (NA49), Inclusive production of charged pions in p+C collisions at 158-GeV/c beam momentum, Eur. Phys. J. C **49**, 897 (2007), arXiv:hep-ex/0606028.

[24] E. Valencia *et al.* (MINERvA), Constraint of the MINERνA medium energy neutrino flux using neutrino-electron elastic scattering, Phys. Rev. D **100**, 092001 (2019), arXiv:1906.00111 [hep-ex].

[25] L. Zazueta *et al.* (MINERvA), Improved constraint on the MINERνA medium energy neutrino flux using ν^{-}e-$\rightarrow\nu^{-}$e- data, Phys. Rev. D **107**, 012001 (2023), arXiv:2209.05540 [hep-ex].

[26] C. Andreopoulos *et al.*, The GENIE Neutrino Monte Carlo Generator, Nucl. Instrum. Meth. A **614**, 87 (2010), arXiv:0905.2517 [hep-ph].

[27] C. H. Llewellyn Smith, Neutrino Reactions at Accelerator Energies, Phys. Rept. **3**, 261 (1972).

[28] D. Rein and L. M. Sehgal, Neutrino Excitation of Baryon Resonances and Single Pion Production, Annals Phys. **133**, 79 (1981).

[29] A. Bodek, I. Park, and U.-k. Yang, Improved low Q**2 model for neutrino and electron nucleon cross sections in few GeV region, Nucl. Phys. B Proc. Suppl. **139**, 113 (2005), arXiv:hep-ph/0411202.

[30] R. A. Smith and E. J. Moniz, NEUTRINO REACTIONS ON NUCLEAR TARGETS, Nucl. Phys. B **43**, 605 (1972), [Erratum: Nucl.Phys.B 101, 547 (1975)].

[31] A. Bodek and J. L. Ritchie, Further Studies of Fermi Motion Effects in Lepton Scattering from Nuclear Targets, Phys. Rev. D **24**, 1400 (1981).

[32] S. Dytman, Neutrino event generators, AIP Conf. Proc. **896**, 178 (2007).

[33] J. Nieves, J. E. Amaro, and M. Valverde, Inclusive quasi-elastic neutrino reactions, Phys. Rev. C **70**, 055503 (2004), [Erratum: Phys.Rev.C 72, 019902 (2005)], arXiv:nucl-th/0408005.

[34] R. Gran, Model Uncertainties for Valencia RPA Effect for MINERvA, (2017), arXiv:1705.02932 [hep-ex].

[35] P. A. Rodrigues *et al.* (MINERvA), Identification of nuclear effects in neutrino-carbon interactions at low three-momentum transfer, Phys. Rev. Lett. **116**, 071802 (2016), [Addendum: Phys.Rev.Lett. 121, 209902 (2018)], arXiv:1511.05944 [hep-ex].

[36] P. Rodrigues, C. Wilkinson, and K. McFarland, Constraining the genie model of neutrino-induced single pion production using reanalyzed bubble chamber data, The European Physical Journal C **76**, 10.1140/epjc/s10052-016-4314-3 (2016).

[37] D. Ruterbories *et al.* (MINERvA), Measurement of inclusive charged-current ν_μ cross sections as a function of muon kinematics at $< E_\nu >\sim 6\ GeV$ on hydrocarbon, Phys. Rev. D **104**, 092007 (2021), arXiv:2106.16210 [hep-ex].

[38] L. Aliaga *et al.* (MINERvA), MINERvA neutrino detector response measured with test beam data, Nucl. Instrum. Meth. A **789**, 28 (2015), arXiv:1501.06431 [physics.ins-det].

[39] G. D'Agostini, A Multidimensional unfolding method based on Bayes' theorem, Nucl. Instrum. Meth. A **362**, 487 (1995).

[40] G. D'Agostini, Improved iterative Bayesian unfolding, in *Alliance Workshop on Unfolding and Data Correction* (2010) arXiv:1010.0632 [physics.data-an].

[41] A. Bashyal, *DUNE and MINERvA Flux Studies and a Measurement of the Charged-Current Quasielastic Antineutrino Scattering Cross Section with* $<E_\nu>\ \tilde{}\ 6\ GeV$ *on a CH Target*, Ph.D. thesis, Oregon State U. (2021).

[42] M. Collaboration, Muon energy scale systematics, `https://cdcvs.fnal.gov/redmine/projects/minerva/wiki/NX_systematics`.

[43] A. Filkins *et al.* (MINERvA), Double-differential inclusive charged-current ν_μ cross sections on hydrocarbon in MINERvA at $\langle E_\nu \rangle \sim 3.5$ GeV, Phys. Rev. D **101**, 112007 (2020), arXiv:2002.12496 [hep-ex].

[44] S. Dytman, Final state interactions in neutrino-nucleus experiments, Acta Phys. Polon. B **40**, 2445 (2009).

[45] S. Dytman, Y. Hayato, R. Raboanary, J. T. Sobczyk, J. Tena Vidal, and N. Vololoniaina, Comparison of validation methods of simulations for final state interactions in hadron production experiments, Phys. Rev. D **104**, 053006 (2021), arXiv:2103.07535 [hep-ph].

[46] S. Henry, H. Su, S. Akhter, Z. Ahmad Dar, V. Ansari, M. V. Ascencio, M. Sajjad Athar, A. Bashyal, M. Betancourt, J. L. Bonilla, A. Bravar, G. A. Díaz, J. Felix, L. Fields, R. Fine, P. K. Gaur, S. M. Gilligan, R. Gran, E. Granados, D. A. Harris, A. L. Hart, J. Kleykamp, A. Klustová, M. Kordosky, D. Last, A. Lozano, X.-G. Lu, S. Manly, W. A. Mann, C. Mauger, K. S. McFarland, M. Mehmood, B. Messerly, J. G. Morfín, D. Naples, J. K. Nelson, C. Nguyen, A. Olivier, V. Paolone, G. N. Perdue, C. Pernas, K.-J. Plows, M. A. Ramírez, R. D. Ransome, N. Roy, D. Ruterbories, H. Schellman, C. J. Solano Salinas, V. S. Syrotenko, E. Valencia, N. H. Vaughan, A. V. Waldron, C. Wret, B. Yaeggy, and L. Zazueta (The MINERvA Collaboration), Measurement of electron neutrino and antineutrino cross sections at low momentum transfer, Phys. Rev. D **109**, 092008 (2024).